



Seismic Source Parameters of Normal-Faulting Inslab Earthquakes in Central Mexico

QUETZALCOATL RODRÍGUEZ-PÉREZ^{1,2,3} and SHRI KRISHNA SINGH¹

Abstract—We studied 62 normal-faulting inslab earthquakes in the Mexican subduction zone with magnitudes in the range of $3.6 \leq M_w \leq 7.3$ and hypocentral depths of $30 \leq Z \leq 108$ km. We used different methods to estimate source parameters to observe differences in stress drop, corner frequencies, source dimensions, source duration, energy-to-moment ratio, radiated efficiency, and radiated seismic energy. The behavior of these parameters is derived. We found that normal-faulting inslab events have higher radiated seismic energy, energy-to-moment ratio, and stress drop than interplate earthquakes as expected. This may be explained by the mechanism dependence of radiated seismic energy and apparent stress reported in previous source parameter studies. The energy-to-moment ratio data showed large scatter and no trend with seismic moment. The stress drop showed no trend with seismic moment, but an increment with depth. The radiated seismic efficiencies showed similar values to those obtained from interplate events, but higher than near-trench events. We found that the source duration is independent of the depth. We also derived source scaling relationships for the mentioned parameters. The low level of uncertainties for the seismic source parameters and scaling relationships showed that the obtained parameters are robust. Therefore, reliable source parameter estimation can be carried out using the obtained scaling relationships. We also studied regional stress field of normal-faulting inslab events. Heterogeneity exists in the regional stress field, as indicated by individual stress tensor inversions conducted for two different depth intervals ($Z < 40$ km and $Z > 40$ km, respectively). While the maximum stress axis (σ_1) appears to be consistent and stable, the orientations of the intermediate and minimum stresses (σ_2 and σ_3) vary over the depth intervals. The stress inversion results showed that the tensional axes are parallel to the dip direction of the subducted plate. At depths greater than 40 km, the maximum horizontal stresses are oblique to the dip direction following the general trend of the slab geometry.

Key words: Inslab earthquakes, seismic source parameters, stress inversion, seismic energy.

1. Introduction

The study of inslab earthquakes in subduction zones is important in understanding the dynamics of the subduction process, the physics of the earthquakes, and the estimation of seismic hazard. The inslab earthquakes are frequently normal-faulting events involving down-dip extension. In Mexico, normal-faulting inslab events can be divided into two main groups based on their epicentral location (PACHECO and SINGH 2010): (1) events below the Altiplano and (2) events near the coast. PACHECO and SINGH (2010) also reported inslab steeply dipping thrust earthquakes at a depth of about 35 km, about 10 km inland from the coast. These events show down-dip compression and are associated with the unbending of the slab (PACHECO and SINGH 2010). Some previous source parameter studies have been conducted for relevant inslab earthquakes in the Mexican subduction zone (e.g. SINGH and WYSS 1976; SINGH *et al.* 1985, 1999, 2000b, 2007, 2014 PÉREZ-CAMPOS *et al.* 2010). These studies were mainly focused on estimating focal mechanisms and seismic source parameters. The first systematic source study for inslab seismicity in the Central Mexico was conducted by GARCÍA *et al.* (2004, 2005). They showed that normal-faulting inslab events have higher stress drops than interplate earthquakes (about four times). GARCÍA *et al.* (2005) showed that ground motions of normal-faulting inslab events have higher amplitudes than interplate earthquakes but their amplitudes decay faster than those of thrust events.

From the perspective of teleseismic data, the radiated seismic energy shows an apparent focal mechanism dependence (CHOY and BOATWRIGHT 1995; PÉREZ-CAMPOS and BEROZA 2001; among others). These studies showed that strike-slip and normal earthquakes generate higher radiated seismic energy

¹ Instituto de Geofísica, Universidad Nacional Autónoma de México, Mexico City, Mexico. E-mail: quetza@geociencias.unam.mx

² Present Address: Centro de Geociencias, Universidad Nacional Autónoma de México, Juriquilla, Querétaro, Mexico.

³ Consejo Nacional de Ciencias y Tecnología, Dirección Adjunta de Desarrollo Científico, Mexico City, Mexico.

than shallow thrust earthquakes. Intermediate depth normal-faulting inslab events have particular characteristics. In a global study based on teleseismic data, CHOY and KIRBY (2004) found that the average apparent stress of these events is considerably higher than for shallow thrust earthquakes. According to TIBI *et al.* (2003) deep earthquake source properties vary with the temperature of the subducting plate. Events in cold slabs show high aftershock activity, high rupture velocity, and high seismic efficiency. In contrast, earthquakes in warm slabs generally have low aftershock productivity, low rupture velocity, and low seismic efficiency. KITA and KATASUMATA (2015) studied intermediate-depth intraslab earthquakes in Japan. Their results show that the median stress drop generally increases with an increase in depth. According to KITA and KATASUMATA (2015), the differences in both the rock rigidity and in the rupture mechanisms could be causes for the stress drop differences within the slab. The systematic estimation of source time functions for many interplate thrust events provides one probe of depth-varying properties in subduction zones (LAY and BILEK 2007). Some authors showed that source duration decreases with depth (e.g. VIDALE and HOUSTON 1993; BOS *et al.* 1998; HOUSTON *et al.* 1998). On the other hand, other studies showed that source duration was almost the same for shallow and deep events (KIKUCHI and ISHIDA 1993) or even anomalously long for intermediate-depth earthquakes (SINGH *et al.* 1996).

The concern about the seismic hazard arises from the fact that in the past many inslab events have caused significant damage to cities in the Mexican Altiplano. Some of these events are the 15 January 1931 (M_w 7.8; $Z = 40$ km) earthquake which caused great destruction to the City of Oaxaca (SINGH *et al.* 1985); the 28 August 1973 (M_w 7.0; $Z = 82$ km) and 24 October 1980 (M_w 7.0; $Z = 60$ km) earthquakes which caused casualties and damage in the states of Puebla, Oaxaca and Veracruz (SINGH and WYSS 1976; YAMAMOTO *et al.* 1984; NAVA *et al.* 1985); the 15 June 1999 (M_w 6.9; $Z = 60$ km) earthquake which caused damage to the City of Puebla (SINGH *et al.* 1999); the 30 September 1999 (M_w 7.4; $H = 40$ km) which caused damage the City of Oaxaca and coastal areas in the state of Oaxaca (SINGH *et al.* 2000b). Recently, the 11 December

2011 (M_w 6.5) was strongly felt in several states along the coast and in Central Mexico, resulting in three fatalities. Some other intermediate size normal-faulting inslab events ($M_w < 6.0$) such as the 13 April 2007 (M_w 5.7), 27 April 2009 (M_w 5.8), 22 May 2009 (M_w 5.6), and the 16 June 2013 (M_w 5.9) have been strongly felt in the Valley of Mexico, especially in Mexico City (SINGH *et al.* 2007, 2014; PÉREZ-CAMPOS *et al.* 2010). In this study, we investigate earthquake source parameters derived from 62 normal-faulting inslab earthquakes using local and regional data. We estimate the focal mechanism and seismic moment (M_o) from moment tensor inversion. We also estimated the source duration (τ), radiated seismic energy (E_R), E_R/M_o ratio, radiated seismic efficiency (η_R), corner frequency (f_c), and source dimensions. We used these measurements together with the moment magnitude for developing seismic source parameter scaling relationships.

2. Data and Methods

2.1. Data

We determined source parameters from 62 intermediate-depth normal-faulting inslab earthquakes ($3.6 \leq M_w \leq 7.3$; $30 \leq Z \leq 108$ km) recorded at local and regional distances (Table 1). The data used consist of recordings from the permanent broadband seismic network of the Mexican National Seismological Service (SSN) and from the stations of the permanent accelerographic networks operated by the Engineering Institute (II), and the National Center for Disaster Prevention (CENAPRED) (Fig. 1). The SSN network is sparse and a typical station consists of a STS-2 seismometer and a Kinematics FBA-23 accelerometer connected to a 24-bit Quanterra digitizer. Both velocity and acceleration channels are sampled at 80 and 100 samples/s. The accelerometric networks mostly consist of Kinematics K2 and ETNA digital accelerographs, equipped with 19- and 18-bit A to D converters, respectively. Accelerograms are available at sampling rates of 80, 100, 200, and 250 Hz. Additionally, we also used data from temporal seismic arrays deployed in Central Mexico. These arrays were operated during various

Table 1
Earthquakes analyzed in this study

Event	Date (yyyy/mm/dd)	Time (hh:mm:ss)	Lat (°E)	Lon (°W)	Depth (km)	M_w	M_o (Nm)	Focal mechanism (strike, dip, rake)	Ref.
1	1994/02/23	18:00:46	17.75	-97.27	75.0	5.80	6.28×10^{17}	(278, 36, -83)	†
						6.10	1.80×10^{18}		2
2	1994/05/23	01:41:52	18.02	-100.57	50.0	6.20	2.77×10^{18}	(273, 39, -76)	†
						6.25	3.02×10^{18}		2
3	1994/12/10	16:17:45	17.98	-101.52	50.0	6.40	5.20×10^{18}	(130, 79, -86)	†
						6.40	5.07×10^{18}		2
4	1995/12/20	21:52:30	18.55	-100.80	77.6	5.30	1.02×10^{17}	(274, 61, -77)	‡
						5.43	1.78×10^{17}		2
5	1996/01/25	12:45:15	18.42	-101.84	59.0	5.50	2.21×10^{17}	(276, 34, -72)	‡
						5.37	1.44×10^{17}		2
6	1996/04/01	03:43:02	16.42	-96.06	57.0	5.20	6.71×10^{16}	(306, 64, -111)	‡
						5.45	1.90×10^{17}		2
7	1996/07/19	09:00:53	17.28	-100.37	44.9	4.73	1.55×10^{16}	(324, 49, -59)	§
						4.90	2.81×10^{16}	(308, 39, -79)	†
						4.70		(320, 34, -59)	
						4.96	3.51×10^{16}		2
8	1997/01/11	20:28:39	18.34	-102.58	40.0	7.01	4.02×10^{19}	(297, 80, -83)	#
						7.10	6.06×10^{19}	(292, 82, -106)	‡
						7.10	5.69×10^{19}		2
9	1997/04/03	21:22:30	17.99	-98.33	33.0	4.99	3.77×10^{16}	(265, 32, -89)	§
						5.20	7.12×10^{16}	(258, 27, -87)	‡
						5.10		(267, 29, -80)	
10	1997/05/22	07:50:54	18.37	-101.87	70.0	4.88	2.66×10^{16}		2
						6.40	4.95×10^{18}	(265, 65, -93)	§
						6.50	6.53×10^{18}	(269, 62, -96)	†
11	1998/04/20	22:59:21	18.35	-101.19	60.0	6.30	3.59×10^{18}		2
						5.85	7.31×10^{17}	(288, 79, -92)	#
						5.90	1.01×10^{18}	(290, 61, -86)	†
12	1998/08/05	16:49:57	17.97	-100.22	55.0	5.90	9.01×10^{17}		2
						4.56	8.74×10^{15}	(344, 38, -68)	§
						4.92	3.05×10^{16}		2
13	1999/06/15	20:42:13	18.13	-97.54	61.0	6.87	2.54×10^{19}	(282, 39, -107)	#
						6.90	3.10×10^{19}	(309, 40, -83)	†
						6.62	1.08×10^{19}		2
14	1999/06/21	17:43:09	18.15	-101.70	60.0	6.22	2.66×10^{18}	(282, 29, -122)	#
						6.30	3.11×10^{18}	(296, 32, -88)	†
						6.10	1.80×10^{18}		2
15	1999/09/30	16:31:23	16.03	-96.96	46.0	7.32	1.21×10^{20}	(305, 47, -66)	#
						7.40	1.72×10^{20}	(300, 49, -78)	†
						7.20	8.03×10^{19}		2
16	1999/12/29	05:19:45	18.04	-101.62	55.0	5.79	5.95×10^{17}	(270, 30, -129)	§
						5.90	8.29×10^{17}	(260, 22, -129)	†
						5.64	3.67×10^{17}		2
17	2000/07/21	06:13:39	18.09	-98.97	50.0	5.71	4.65×10^{17}	(294, 31, -91)	1
						5.90	7.14×10^{17}	(305, 32, -80)	†
						5.80	7.14×10^{17}	(289, 33, -81)	‡
						5.90		(295, 28, -88)	
18	2001/02/11	00:35:52	18.38	-101.60	50.0	5.68	4.22×10^{17}		2
						4.64	1.13×10^{16}	(286, 62, -73)	1
						4.90	2.85×10^{16}		2
19	2001/03/05	10:17:36	17.13	-100.06	41.0	5.02	4.28×10^{16}	(290, 13, -91)	1
						5.30	1.00×10^{17}	(338, 15, -63)	†
						5.10		(250, 16, -131)	
						5.44	1.84×10^{17}		2

Table 1 continued

Event	Date (yyyy/mm/dd)	Time (hh:mm:ss)	Lat (°E)	Lon (°W)	Depth (km)	M_w	M_0 (Nm)	Focal mechanism (strike, dip, rake)	Ref.
20	2001/03/06	21:57:56	17.14	-100.10	37.0	4.91	2.91×10^{16}	(336, 41, -39)	1
						5.20	8.30×10^{16}	(336, 37, -64)	†
						5.00		(340, 30, -49)	
21	2002/01/30	08:42:07	18.22	-95.94	107.0	5.28	1.06×10^{17}		2
						5.87	7.96×10^{17}	(329, 58, -85)	1
						5.90	9.43×10^{17}	(317, 63, -94)	†
22	2002/06/27	04:59:49	17.78	-100.46	50.0	5.92	9.66×10^{17}		2
						4.37	4.41×10^{15}	(292, 67, -89)	1
						4.71	1.48×10^{16}		2
23	2002/12/10	03:09:33	17.75	-101.27	46.0	5.41	1.64×10^{17}	(201, 17, -40)	§
						5.30		(220, 15, -15)	
						5.36	1.40×10^{17}		2
24	2003/04/21	07:56:26	17.50	-101.26	35.8	4.39	4.71×10^{15}	(215, 25, -17)	§
						4.50		(210, 37, -15)	
						4.77	1.82×10^{16}		2
25	2003/05/16	09:09:24	18.29	-101.26	60.0	4.85	2.33×10^{16}	(290, 60, -74)	1
						5.00	3.70×10^{16}	(297, 56, -61)	‡
						4.70		(292, 67, -79)	
26	2003/07/21	23:53:44	18.44	-101.02	65.0	4.90	2.85×10^{16}		2
						5.04	4.52×10^{16}	(270, 57, -114)	1
						5.10	6.40×10^{16}	(289, 52, -89)	‡
27	2003/11/19	13:50:28	17.86	-99.54	50.0	4.90		(134, 37, -54)	
						5.20	8.03×10^{16}		2
						5.03	4.31×10^{16}	(295, 30, -46)	1
28	2004/01/17	21:13:09	17.70	-95.64	108.0	5.20	8.89×10^{16}	(277, 37, -69)	‡
						5.10		(306, 44, -52)	
						5.18	7.50×10^{16}		2
29	2004/08/07	11:49:13	17.25	-95.30	100.0	5.09	5.45×10^{16}	(330, 45, -70)	1
						5.20	7.19×10^{16}	(325, 44, -77)	‡
						5.12	6.09×10^{16}		2
30	2004/10/28	20:30:02	18.47	-99.80	54.2	5.70	4.40×10^{17}	(324, 57, -97)	1
						5.80	5.35×10^{17}	(312, 66, -103)	‡
						5.71	4.68×10^{17}		2
31	2004/11/22	03:49:25	17.99	-99.63	54.0	4.85	2.34×10^{15}	(346, 38, -94)	§
						4.80		(176, 49, -89)	
						4.95	3.39×10^{16}		2
32	2004/05/26	15:55:56	17.94	-99.98	58.0	4.45	5.95×10^{15}	(294, 34, -60)	§
						4.30		(304, 38, -50)	
						4.48	6.68×10^{15}		2
33	2005/05/26	15:55:56	17.94	-99.98	58.0	4.71	1.44×10^{16}	(291, 37, -81)	1
						4.60		(289, 34, -76)	
						4.87	2.57×10^{16}		2
34	2005/09/08	16:02:02	17.33	-101.36	28.0	4.07	1.61×10^{15}	(220, 23, -146)	1
						4.73	1.58×10^{16}		2
						4.91	2.88×10^{16}	(328, 69, -45)	1
35	2005/09/24	01:14:02	17.88	-97.03	106.0	5.00	3.70×10^{16}	(353, 41, -78)	‡
						5.13	6.31×10^{16}		2
						4.73	1.55×10^{16}	(279, 70, -85)	1
36	2005/12/14	21:22:36	18.39	-101.21	46.0	4.90	2.78×10^{16}	(267, 60, -97)	‡
						4.97	3.63×10^{16}		2
						4.37	4.49×10^{15}	(307, 35, -63)	§
37	2006/06/26	15:49:18	18.05	-100.01	56.4	4.30		(293, 35, -79)	
						4.63	1.12×10^{16}		2
						4.65	1.19×10^{16}	(344, 20, -60)	1
37	2006/07/07	17:43:34	15.78	-96.26	31.0	4.90	2.85×10^{16}		2

Table 1 continued

Event	Date (yyyy/mm/dd)	Time (hh:mm:ss)	Lat (°E)	Lon (°W)	Depth (km)	M_w	M_0 (Nm)	Focal mechanism (strike, dip, rake)	Ref.
38	2006/08/11	14:30:44	18.45	-101.30	55.0	5.86	7.89×10^{17}	(300, 66, -72)	1
						6.00	1.26×10^{18}	(283, 57, -87)	‡
						5.60	3.20×10^{17}		2
39	2006/12/17	03:17:50	17.91	-101.31	58.0	4.81	2.05×10^{16}	(232, 47, -132)	1
						5.12	6.09×10^{16}		2
40	2007/01/27	11:22:10	18.07	-102.13	30.0	4.21	2.59×10^{15}	(303, 45, -5)	1
						4.22	2.72×10^{15}		2
41	2007/02/14	18:04:40	16.75	-96.18	75.0	4.69	1.34×10^{16}	(341, 71, -67)	1
						4.80	2.02×10^{16}		2
42	2007/05/04	10:21:10	17.20	-96.84	65.0	4.97	2.59×10^{16}	(320, 55, -115)	1
						5.00	4.57×10^{16}	(302, 59, -125)	‡
						5.19	7.76×10^{16}		2
43	2007/07/28	13:45:24	18.05	-100.84	50.0	4.96	3.46×10^{16}	(307, 45, -86)	1
						5.10	6.47×10^{16}	(312, 40, -85)	‡
						5.20	8.03×10^{16}		2
44	2007/11/26	21:56:12	18.65	-101.70	60.0	5.67	3.98×10^{17}	(257, 63, -112)	1
						5.70	4.66×10^{17}	(326, 72, -82)	‡
						5.65	3.80×10^{17}		2
45	2008/04/05	06:27:50	17.91	-97.91	55.0	3.97	1.12×10^{15}	(304, 58, -78)	1
						4.20	2.54×10^{15}		2
46	2008/04/15	07:31:43	18.31	-101.01	55.0	4.59	9.65×10^{15}	(307, 69, -91)	1
						4.84	2.32×10^{16}		2
47	2008/04/28	00:06:29	18.05	-100.01	48.0	5.60	5.32×10^{17}	(317, 34, -68)	1
						5.80	7.00×10^{17}	(317, 48, -85)	‡
						5.40		(138, 40, -88)	
48	2008/04/29	10:56:42	18.47	-101.19	65.0	5.75	5.37×10^{17}		2
						5.29	1.07×10^{17}	(262, 60, -94)	1
						5.30	1.10×10^{17}	(275, 62, -86)	‡
49	2008/12/15	14:27:10	17.07	-97.00	65.0	5.28	1.06×10^{17}		2
						4.42	5.31×10^{15}	(323, 47, -92)	1
50	2009/01/14	17:04:35	18.10	-100.07	47.0	4.53	7.94×10^{15}		2
						4.16	2.16×10^{15}	(322, 38, -75)	1
51	2009/05/22	19:24:17	18.10	-98.43	50.0	4.35	4.26×10^{15}		2
						5.55	2.67×10^{17}	(280, 37, -76)	1
52	2009/08/15	13:22:45	18.06	-100.67	60.0	5.60	3.71×10^{17}	(282, 34, -63)	‡
						5.67	4.07×10^{17}		2
						5.39	1.51×10^{17}	(291, 48, -64)	1
53	2010/08/22	07:06:55	18.22	-100.91	50.0	5.50	2.08×10^{17}	(276, 43, -70)	‡
						5.45	1.90×10^{17}		2
						4.01	1.28×10^{15}	(300, 62, -74)	1
54	2010/08/31	12:52:55	18.12	-100.45	50.0	4.10	1.80×10^{15}		2
						3.63	3.50×10^{14}	(292, 43, -64)	1
55	2010/09/28	08:46:33	18.18	-102.38	65.0	4.00	1.27×10^{15}		2
						3.95	1.05×10^{15}	(285, 71, -105)	1
56	2011/12/11	01:47:25	17.85	-99.98	55.0	4.20	2.54×10^{15}		2
						6.38	4.79×10^{18}	(299, 29, -78)	1
57	2012/02/05	17:01:11	18.37	-101.43	60.0	6.50	6.06×10^{18}	(284, 34, -84)	‡
						6.50	7.16×10^{18}		2
						4.75	1.64×10^{16}	(272, 59, -94)	1
58	2012/04/02	17:36:42	16.27	-98.47	16.0	4.90	2.85×10^{16}		2
						5.94	1.01×10^{18}	(271, 50, -65)	1
59	2012/11/15	09:20:22	18.17	-100.52	46.0	6.10	1.52×10^{18}	(272, 58, -87)	‡
						6.00	1.27×10^{18}		2
						6.02	1.32×10^{18}	(303, 38, -74)	1
						6.10	1.61×10^{18}	(297, 39, -80)	‡
						6.00	1.27×10^{17}		2

Table 1 continued

Event	Date (yyyy/mm/dd)	Time (hh:mm:ss)	Lat (°E)	Lon (°W)	Depth (km)	M_w	M_o (Nm)	Focal mechanism (strike, dip, rake)	Ref.
60	2013/01/30	07:24:10	16.39	−96.21	46.0	4.03	1.38×10^{15}	(192, 44, −83)	1
						4.40	5.07×10^{15}		2
61	2013/06/16	05:19:03	18.04	−99.25	54.0	5.72	4.79×10^{17}	(311, 33, −64)	1
						5.90	7.80×10^{17}	(311, 33, −73)	‡
						5.90	9.01×10^{17}		2
62	2013/08/26	23:19:35	18.23	−100.78	46.0	4.31	3.67×10^{15}	(316, 64, −72)	1
						4.47	6.46×10^{15}		2

All locations are based on local/regional data

† Location and depth from local and regional data reported by GARCÍA *et al.* (2004). M_o and focal mechanism from Harvard CMT

‡ Location, depth, M_o , M_w , focal mechanism from Harvard CMT

§ Location from PACHECO and SINGH (2010). M_o , M_w , depth, and focal mechanism from regional moment tensor (this study)

|| Focal mechanism and M_w from PACHECO and SINGH (2010)

Location from local and regional data reported by GARCÍA *et al.* (2004). M_o , M_w , depth and focal mechanism from regional moment tensor (this study)

1 Location local and regional data from the Mexican CMT catalog of the Universidad Nacional Autónoma de México (UNAM). M_o , M_w , depth, and focal mechanism from regional moment tensor (this study)

2 M_w and M_o from S-wave spectra of local and regional recordings

experiments: the Colima Volcano deep seismic experiment (CODEX), the Mapping of the Rivera subduction zone (MARS), the Meso-American subduction experiment (MASE), and the Veracruz-Oaxaca line (VEOX) (Fig. 1). The CODEX network consists of Guralp CMG 40T sensors with Quanterra digitizers at sampling rates of 100 samples/s. The MARS array consists of a STS-2 seismometer with Quanterra digitizer at sampling rates of 40 samples/s. The MASE and VEOX arrays have all Guralp 3T broadband sensors (120 s to 50 Hz). Figure 2 shows epicenters of the studied events in Central Mexico.

2.2. Data Processing

We processed all recordings in the same fashion for estimating radiated seismic energy and for the spectral analysis. The digital time series of the events are corrected for baseline and for instrument response. The horizontal components of accelerographs and/or seismometers at each station are windowed. The window length was chosen such that it included the main S-wave arrival and a point at which 95 % of the shear energy was contained in the

window. The signals are then Fourier transformed by a fast Fourier transform and a 10 % cosine tapering window is applied at both ends of the signal. Depending on the analysis, the velocity and acceleration time series are integrated to obtain a velocity or displacement spectrum of the signal (see next section). The spectra are not smoothed. For spectral source parameter estimation, we compute an average spectrum of both horizontal components before modeling the seismic source.

3. Source Parameter Estimation

3.1. Regional Moment Tensor Inversion

Long-period seismic waves recorded at regional distances have been used to extract information about the earthquake source: specifically, seismic moment, focal mechanism, and centroid depth. The use of seismic waves at longer periods improves the estimation of earthquake source parameters because they are relatively insensitive to the effects of lateral velocity and density heterogeneities (RITSEMA and

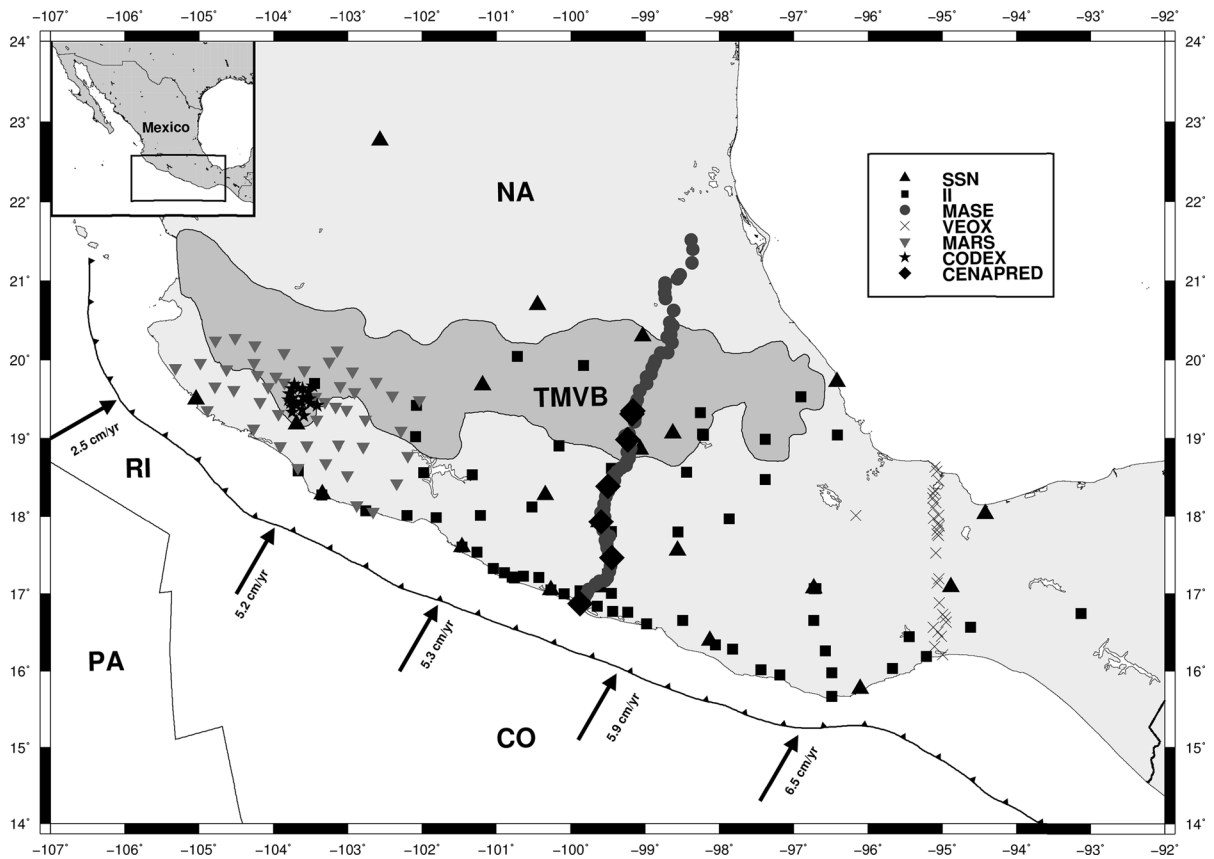


Figure 1

Main tectonic features of Central Mexico. NA is the North American plate, CO is the Cocos plate, PA is the Pacific plate, RI is the Rivera microplate, and TMVB is the Transmexican volcanic belt. *Arrows* show the convergence rate of the RI and CO plates with respect to the NA. *Symbols in the box* show the stations of the Mexican National Seismological Service (SSN), Engineering Institute (II), and the National Center for Disaster Prevention (CENAPRED), the Meso-American subduction experiment (MASE), the Veracruz-Oaxaca line (VEOX), the Mapping the Rivera subduction zone (MARS) and the Colima Volcano deep seismic experiment (CODEX) arrays

LAY 1995). We used the matrix inversion method (e.g., ICHINOSE *et al.* 2003, 2014) to invert for the point source moment tensor using Green's functions computed for a 1D velocity model based on the methodology presented by JOST and HERRMANN (1989). The method incorporates modifications (based on HERRMANN and HUTCHENSEN 1993; MINSON and DREGER 2008) needed to calculate full moment tensors (6-degree of freedom) that include isotropic components. Commonly the inversion involves solving for the deviatoric moment tensor, which is suitable for tectonic earthquakes. In this study, the inversion is done imposing a deviatoric moment tensor without isotropic component which is a

recommended setting for all tectonic sources (ICHINOSE 2014).

The Green's functions are computed using a fast reflectivity and frequency wave number ($f-k$) summation technique (ZENG and ANDERSON 1995). For the computation of the Green's functions, we used the 1D crustal model reported by CAMPILLO *et al.* (1996). The Green's functions are computed using different depth increments (from 2 to 5 km). To account for any origin time (OT) and location errors, the synthetics are shifted relative to the observed time by changing the OT few seconds before/after the final location OT during the inversion. The shift that produces the best fit is used in the final solution. The maximum value of

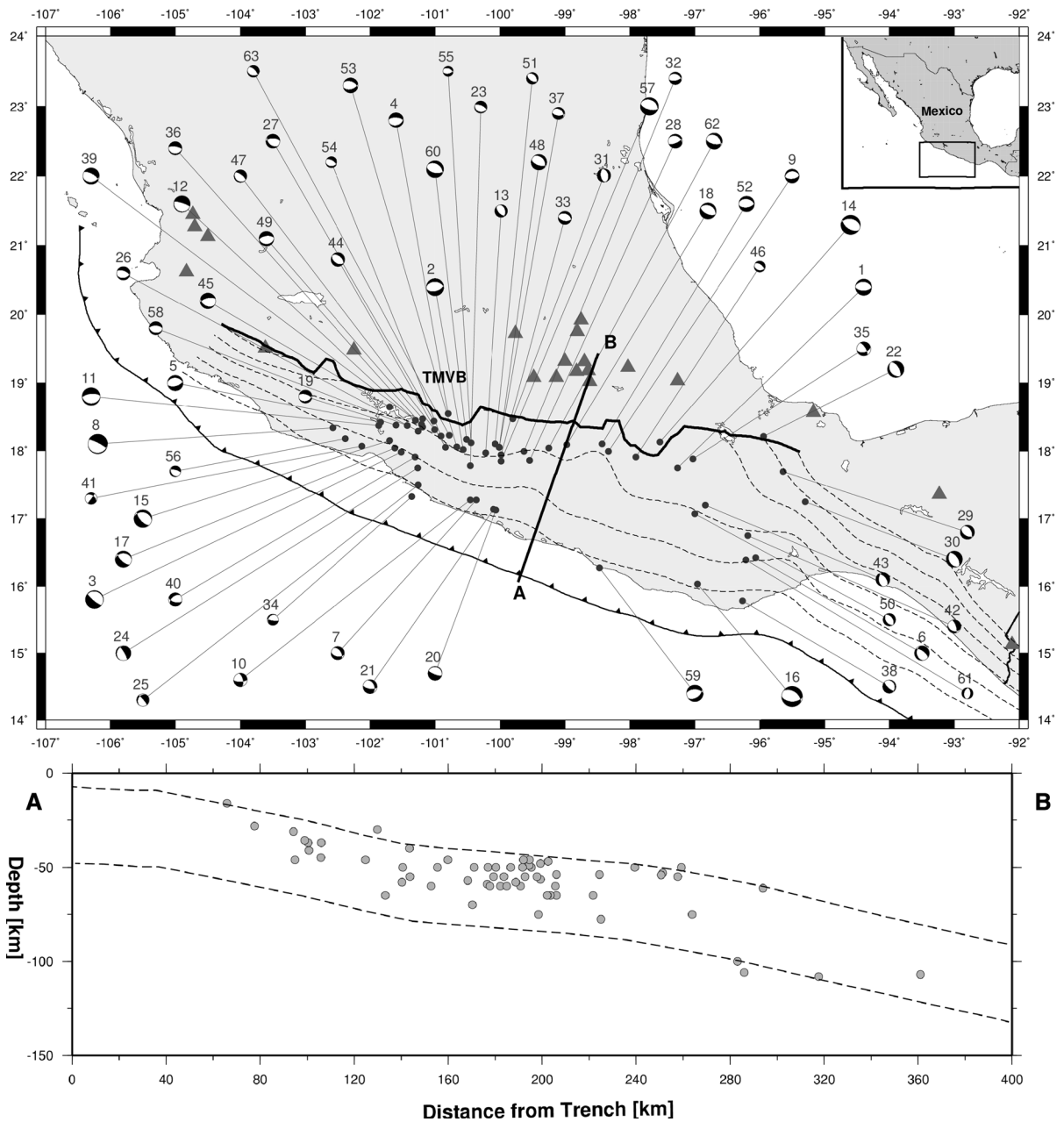


Figure 2

Normal-faulting in-slab events in Central Mexico ($3.9 < M_w < 7.1$). Numbers indicate the events in Table 1. Gray triangles are volcanoes and the black-bold line delimits the boundary of the TMVB. Dashed lines show contour lines of the subducted slab at 20, 40, 60, 80 and 120 km depth (upper panel). Section along AB (lower panel). Dashed lines indicate plate interfaces. Locations of in-slab earthquakes are indicated. The dashed lines delineate the subducted Cocos plate (lower panel)

time shift for synthetic data was set to be 3 s. The allowed time shift is large enough to make up for small hypocentral errors, but small enough to

disallow cycle skipping that could produce erroneous mechanisms. The preferred solution is obtained by a simple grid search over the focal depths and also over

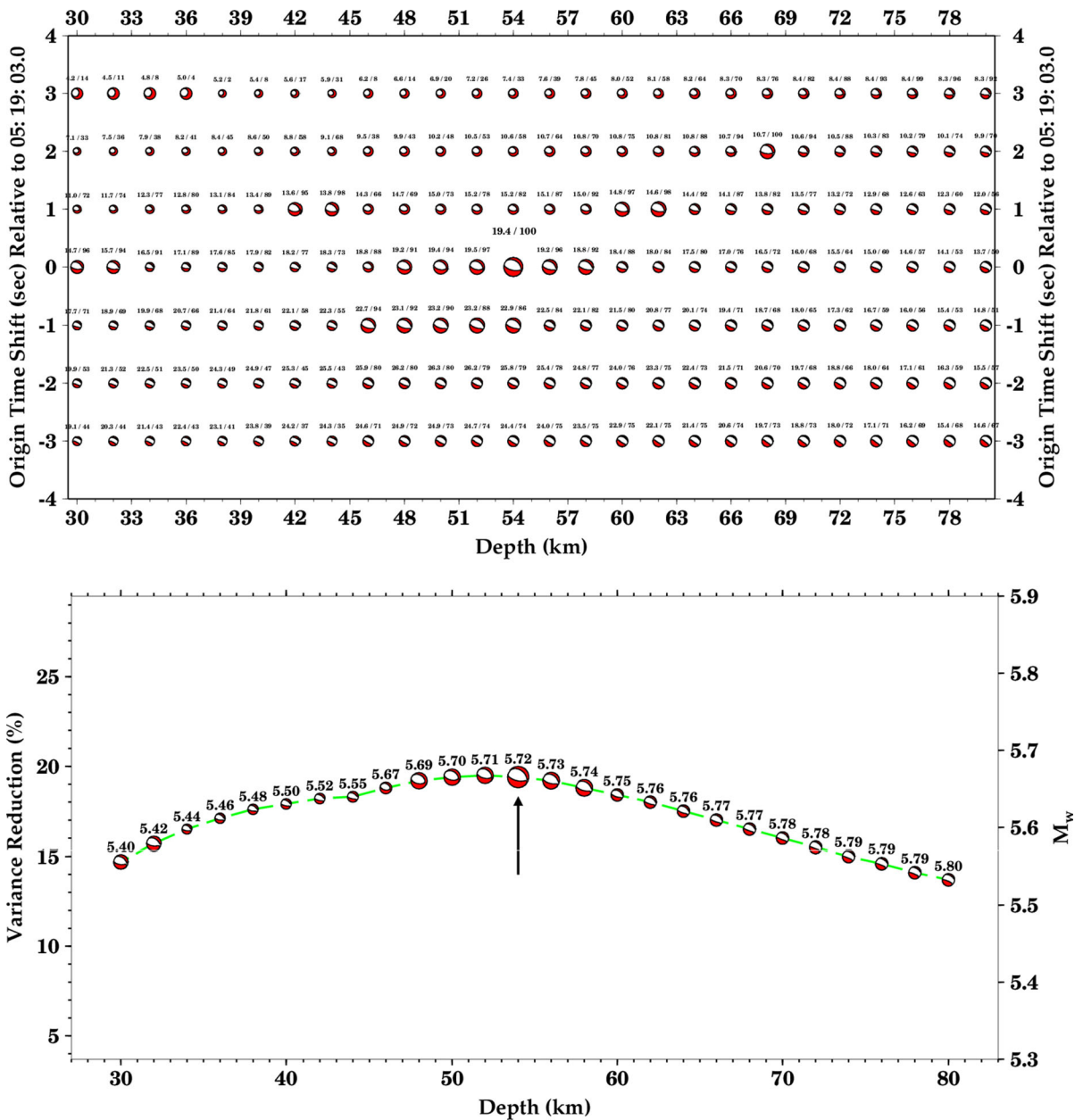
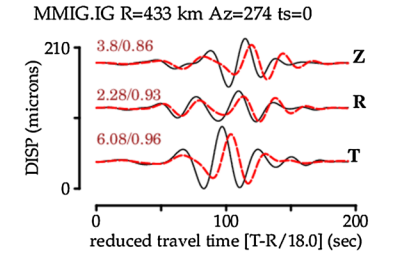
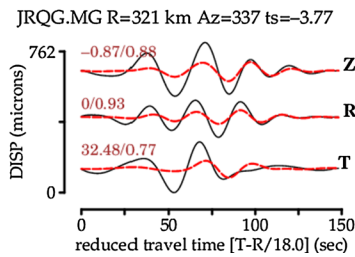
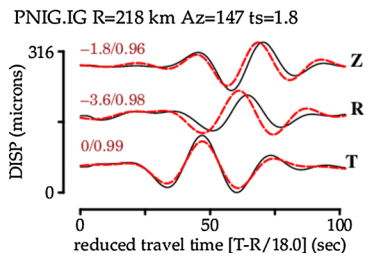
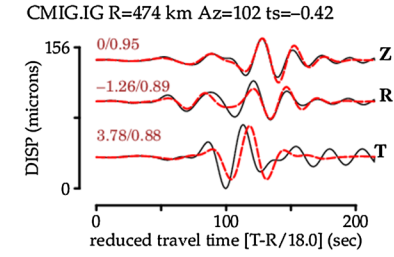
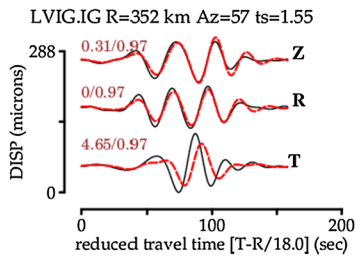
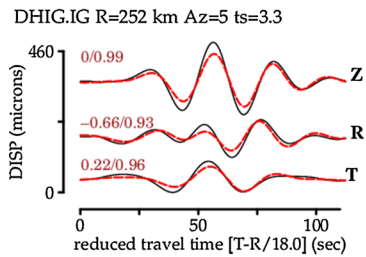
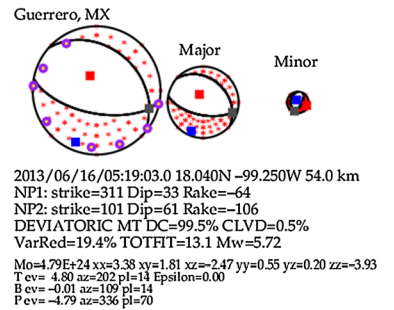
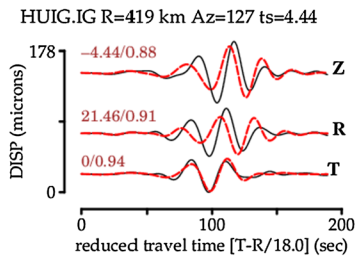
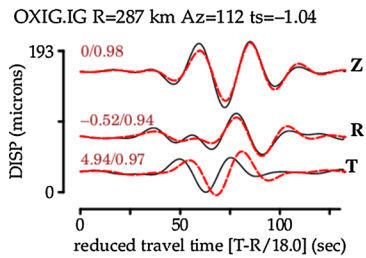
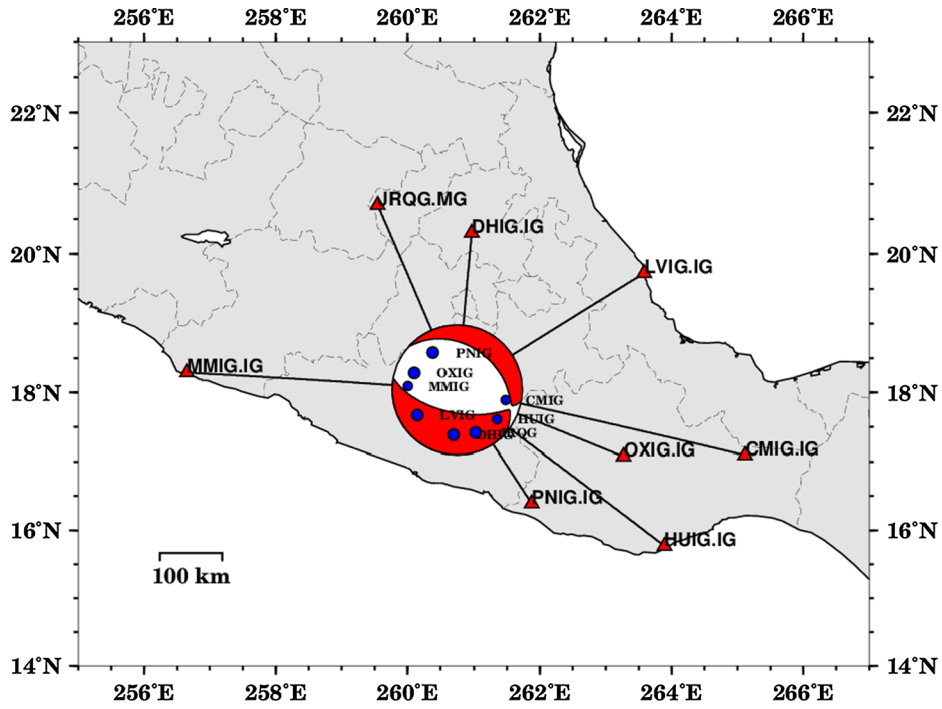


Figure 3

Moment tensor inversion results for event 61 using a simple grid search scheme. The moment tensors as a function of depth and origin time are shown with the moment tensors scaled as a function of L2 norm error in the waveform misfits (larger moment tensors signify smaller errors). We perform a grid search to solve for the best fitting origin time and focal depth by iterating the moment tensor inversion. The best fitting depth is 54 km, and origin time is 16 June 2013 05:19:03 UTC (*upper panel*). Goodness of the focal mechanism fit as function of source depth; mechanisms are plotted each 2 km (*lower panel*)

the origin time (Figs. 3, 4 show an example). The solution that has the highest percentage of variance reduction and double couple component is selected

(Figs. 3, 4 show an example). Records from stations relatively close to the epicenter are discarded to avoid finite fault effects, and stations far from the epicenter



◀Figure 4

Example of moment tensor solution (16 June 2013 earthquake). Comparison between observed (*black lines*) and synthetic (*red lines*) displacement waveforms for the preferred focal mechanism obtained from the moment tensor inversion. The epicentral distance (R) and azimuth (Az) of each station is written above their traces. Z, R, T indicates vertical, radial, and transverse components, respectively

are discarded to ensure good signal to noise ratio. We integrated the records to obtain displacements and filter them using different frequency bands depending on their magnitudes (Table 2) following PÉREZ-CAMPOS *et al.* (2010).

3.2. Estimation of Radiated Seismic Energy

We estimated the radiated seismic energy (E_R) by integrating squared velocity spectra following SINGH and ORDAZ (1994); E_R is defined by

$$E_R = [4\pi R^2 \{G^2(R)/R^2\} \rho \beta / F^2] 2 \times \int_0^\infty \{V_N^2(f) + V_E^2(f) + V_Z^2(f)\} e^{2\pi f R / \beta Q(f)} df, \quad (1)$$

where $V_j(f)$ is the velocity spectrum of the j th component of the S-wave group, R is the hypocentral distance; $G(R)$ is the geometrical spreading correction which may be taken as $G(R) = R^{-1}$ for inslab Mexican earthquakes (GARCÍA *et al.* 2004); ρ and β are the density and shear velocity in the focal region, respectively; F is the free-surface amplification (2.0), and $Q(f)$ is the quality factor taken here as $Q(f) = 251f^{0.58}$ (GARCÍA *et al.* 2004). The stations used in this study are all situated on rock sites. For this reason, we applied the site effect correction for a generic rock site (BOORE and JOYNER 1997).

Table 2

Frequency bands used in the moment tensor inversion

Magnitude	Distance (km)	Frequency band (Hz)
$3.5 \leq M < 5.0$	$30 < R < 400$	0.02–0.05
$5.0 \leq M < 6.5$	$100 < R < 600$	0.01–0.05
$6.5 \leq M < 7.5$	$200 < R < 995$	0.01–0.05
$7.5 \leq M$	$500 < R < 995$	0.005–0.02

Following PÉREZ-CAMPOS *et al.* (2003), we applied site corrections using the combined effect of frequency-dependent site amplification and site attenuation, defined as $A(f) = A_o(f) e^{-\pi \kappa f}$, where $A_o(f)$ is the amplification factor and κ is the attenuation parameter (Anderson and Hough 1984; BOORE and JOYNER 1997). Additionally, we used an average attenuation parameter appropriate for the station obtained from previous studies (CASTRO *et al.* 1990; HUMPHREY and ANDERSON 1992). In case the value of κ is unknown, we used an average value of $\kappa = 0.0306$ s (CASTRO *et al.* 1990; HUMPHREY and ANDERSON 1992) as used by PÉREZ-CAMPOS *et al.* (2003).

Table 3 shows results for the analyzed events. Figure 5 shows an example of the E_R estimation as function of distance. The E_R estimations are used to derive a scaling relationship between E_R and M_o . We also used the estimated M_o from the regional moment tensor inversion to determine the E_R/M_o ratio (Fig. 6). The E_R/M_o ratio is different for different types of earthquakes (VENKATARAMAN and KANAMORI 2004). For example, the ratio takes values of 7×10^{-7} to 3×10^{-6} for tsunami earthquakes; 5×10^{-6} to 2×10^{-5} for interplate and downdip earthquakes; 2×10^{-5} to 3×10^{-4} for intraplate deep and crustal earthquakes (VENKATARAMAN and KANAMORI 2004). We calculated radiated efficiency, (η_R), which is defined as $\eta_R = E_R / (E_R + E_G)$ $\sim 2(E_R/M_o) / (\Delta\sigma_s / \mu)$, where E_G is the fracture energy, and $\Delta\sigma_s$ is the static stress drop (HUSSEINI 1977) (Fig. 7). We followed KEILIS-BOROK (1959) to estimate static stress as $\Delta\sigma_s = 7M_o/16r^3$. VENKATARAMAN and KANAMORI (2004) reported that η_R of most earthquakes lies between 0.25 and 1.0. Deep earthquakes have also small radiation efficiencies (VENKATARAMAN and KANAMORI 2004).

3.3. Source Spectra

We estimated source displacement and acceleration spectra, $\dot{M}(f)$ and $f^2\dot{M}(f)$, of the earthquakes from the analysis of the S-wave group recorded at hard sites following BOORE (1983) and SINGH and ORDAZ (1994). The Fourier acceleration spectral amplitude of the intense part of the ground motion

Table 3
Source parameter estimation

Event	E_R (Nm)	E_R/M_0	$\Delta\sigma$ (bars)	f_c (Hz)	f_{max} (Hz)	r (km)	η_R	n	τ_p (s)	τ_t (s)
1	3.71×10^{13}	5.91×10^{-5}	353	0.62	10.15	2.93	0.487	1	1.60	
2*	2.56×10^{14}	9.26×10^{-5}	324	0.85 [#]	7.11	3.33	0.254	2	1.70	4.3 [†]
			324	0.52 [#]						
3*	1.19×10^{15}	2.29×10^{-4}	515	0.33	9.63	5.82	1.786	2	1.70	6.5 [‡]
			494	0.49 [#]						
4	5.33×10^{12}	5.22×10^{-5}	152	1.03	9.41	1.78	0.594	1	1.00	
5	1.39×10^{13}	6.29×10^{-5}	167	1.12	7.85	1.59	0.235	1	1.30	
6	8.37×10^{12}	1.25×10^{-4}	520	1.53	12.54	1.15	0.583	1	0.90	
7	9.25×10^{11}	5.97×10^{-5}	326	2.29	14.31	0.80	0.406	1	0.50 [‡]	
			310	2.73 [#]					0.40 [*]	
8*	3.68×10^{15}	9.16×10^{-5}	338	0.21	5.51	8.46	0.284	3	4.80	13.5
			266	0.17 [#]						
9	7.32×10^{11}	1.94×10^{-5}	136	1.81	9.78	0.97	0.097	1	0.75	
10*	3.36×10^{14}	6.79×10^{-5}	240	0.39	7.01	4.49	0.255	1	0.70 [*]	4.00
			221	0.34 [#]						
11	6.76×10^{13}	9.25×10^{-6}	235	0.67	6.58	2.67	0.005	1	3.00	
			206	0.63 [#]						
12	5.51×10^{11}	6.31×10^{-5}	205	2.04	12.91	0.87	0.978	1	0.40	
13	2.64×10^{15}	1.04×10^{-4}	882	0.46	7.02	4.07	0.057	3	4.20	8.0
			733	0.31 [#]						
14	2.79×10^{14}	1.05×10^{-4}	473	0.71	6.96	2.46	0.121	1	2.20	
			303	0.49 [#]						
15*	8.51×10^{15}	7.03×10^{-5}	665	0.22	7.02	7.85	0.058	3	6.00	14.5 [§]
			660	0.17 [#]						
16	4.96×10^{13}	8.34×10^{-5}	176	0.83	12.74	2.11	0.271	1	1.43	
			128	0.57 [#]						
17	4.27×10^{13}	9.19×10^{-5}	255	0.90	8.52	1.93	0.292	1	1.34	
			258	0.76 [#]					1.30 [*]	
18	1.16×10^{12}	1.03×10^{-4}	377	0.81 ¹	12.52	0.87	1.234	1	0.50	
			185	2.01					0.40 [*]	
19	9.89×10^{12}	2.31×10^{-4}	184	1.10	13.35	1.60	4.548	1	0.70	
			151	1.22 [#]					0.60 [*]	
20	4.72×10^{12}	1.62×10^{-4}	247	1.44	12.71	1.28	2.402	1	0.60	
			230	1.50 [#]					0.50 [*]	
21	2.39×10^{14}	3.01×10^{-4}	1389	1.18	7.46	1.77	0.431	1	1.56	
			1981	1.36 [#]						
22	1.24×10^{11}	2.82×10^{-5}	232	2.73	11.63	0.66	0.378	1	0.36	
23	8.31×10^{12}	5.06×10^{-5}	440	1.61	10.06	1.09	0.082	1	1.00	
									0.90 [*]	
24	2.52×10^{11}	5.36×10^{-5}	293	2.71	14.25	0.67	0.704	1	0.36	
25	8.76×10^{11}	3.76×10^{-5}	172	1.94	11.48	0.90	0.242	1	0.35 [*]	
									0.58	
26	2.13×10^{12}	4.71×10^{-5}	315	1.72	10.60	1.03	0.234	1	0.70	
27	3.71×10^{12}	8.61×10^{-5}	327	1.76	10.66	1.03	0.449	1	0.68	
									0.65 [*]	
28	1.93×10^{12}	3.55×10^{-5}	338	1.88	8.88	0.96	0.118	1	0.74	
29	1.80×10^{14}	4.09×10^{-4}	872	1.33	8.06	1.33	0.450	1	1.30	
30	1.07×10^{12}	4.57×10^{-4}	275	2.17	15.04	0.82	2.152	1	0.30	
									0.30 [*]	
31	1.54×10^{11}	2.58×10^{-5}	283	3.62	13.52	0.50	0.111	1	0.40	
32	2.95×10^{12}	2.05×10^{-4}	269	2.35	12.16	0.75	1.235	1	0.40 [*]	
									0.50	

Table 3 continued

Event	E_R (Nm)	E_R/M_0	$\Delta\sigma$ (bars)	f_c (Hz)	f_{max} (Hz)	r (km)	η_R	n	τ_p (s)	τ_t (s)
33	2.13×10^{11}	1.32×10^{-4}	303	2.81	15.14	0.66	4.849	1	0.28	
34	4.78×10^{12}	1.66×10^{-4}	370	1.95	11.19	0.91	0.893	1	0.30*	0.70
35	8.40×10^{11}	5.42×10^{-5}	294	2.11	12.05	0.86	0.457	1	0.40*	0.50
36	3.30×10^{11}	7.35×10^{-5}	195	2.77	15.55	0.65	0.925	1	0.50*	0.35
37	2.48×10^{12}	2.09×10^{-4}	178	1.33	14.02	1.34	8.693	1	0.48	0.50*
38	9.84×10^{12}	1.25×10^{-5}	310	1.95	6.97	0.96	0.003	1	1.60	
39	3.03×10^{12}	1.48×10^{-4}	177	1.55	13.96	1.15	2.259	1	0.55	
40	1.37×10^{11}	5.28×10^{-5}	170	4.10	14.48	0.43	0.333	1	0.30	0.30*
41	6.17×10^{11}	4.60×10^{-5}	287	2.33	14.26	0.80	0.361	1	0.50	
42	2.73×10^{12}	1.05×10^{-4}	226	1.53	14.41	1.19	1.405	1	0.60	
43	7.98×10^{12}	2.31×10^{-4}	164	1.31	13.98	1.44	4.101	1	0.64	0.70*
44	1.59×10^{14}	4.00×10^{-4}	320	1.03	7.42	0.48	0.023	1	1.28	
45	6.02×10^{10}	5.38×10^{-5}	111	3.59	14.06	0.48	1.093	1	0.24	0.25*
46	4.96×10^{11}	5.14×10^{-5}	180	2.12	14.78	0.86	0.697	1	0.44	0.45*
47	5.06×10^{13}	9.50×10^{-5}	348	0.93	7.71	1.93	0.264	1	1.40	1.20*
48	6.40×10^{12}	5.98×10^{-5}	293	1.48	9.93	1.20	0.199	1	0.88	
49	3.14×10^{11}	5.92×10^{-5}	356	3.80	13.17	0.49	0.270	1	0.38	
50	1.24×10^{11}	5.75×10^{-5}	360	4.62	15.43	0.39	0.325	1	0.30	0.30*
51	2.76×10^{13}	1.04×10^{-4}	441	1.09	8.60	1.63	0.347	1	1.66	1.60*
52	1.22×10^{13}	8.05×10^{-5}	447	1.06 ¹	10.12	1.35	0.270	1	0.98	
53	4.82×10^{10}	3.76×10^{-5}	412	1.40	15.57	0.35	0.259	1	0.25	0.20*
54	8.02×10^9	2.29×10^{-5}	222	5.23	16.82	0.48	1.488	1	0.17	0.20*
55	7.50×10^9	7.14×10^{-6}	164	3.64	15.12	0.48	0.155	1	0.24	
56*	5.80×10^{14}	1.21×10^{-4}	177	3.69	15.12	0.48	0.155	1	9.0	4.00*
57	9.44×10^{11}	5.76×10^{-5}	625	7.81	2.58	0.089	2	4.40	0.24	
58	5.01×10^{14}	4.96×10^{-4}	0.69	7.81	2.58	0.089	2	4.40	0.52	1.50*
59	1.16×10^{14}	8.77×10^{-5}	216	2.03	13.77	0.90	0.527	1	1.67	1.80
60	1.00×10^{11}	7.29×10^{-5}	341	0.65	7.82	2.67	1.923	1	2.00*	2.00*
61	5.19×10^{13}	1.08×10^{-4}	456	0.72	7.69	2.47	0.206	1	0.25	0.20*
			414	0.65 ¹	15.58	0.39	0.644	1	1.35	
			387	4.56	8.60	2.27	0.542	1	1.40*	
			368	0.79	8.60	2.27	0.542	1		
			391	0.80 ¹						

Table 3 *continued*

Event	E_R (Nm)	E_R/M_o	$\Delta\sigma$ (bars)	f_c (Hz)	f_{max} (Hz)	r (km)	η_R	n	τ_p (s)	τ_t (s)
62	3.51×10^{10}	9.55×10^{-6}	131	2.56	14.00	0.79	0.264	1	0.34	0.30 [*]

† COCCO et al. (1997), source duration from regional and local data

‡ SINGH et al. (2000a), source duration from regional and local data

§ SINGH et al. (2000b), source duration from regional and local data

|| This study, source duration from moment tensor inversion with local and regional data

* This study, source duration from near source records

$\Delta\sigma$ and f_c from GARCÍA et al. (2004)

1 $\Delta\sigma$ and f_c from SINGH et al. (2014)

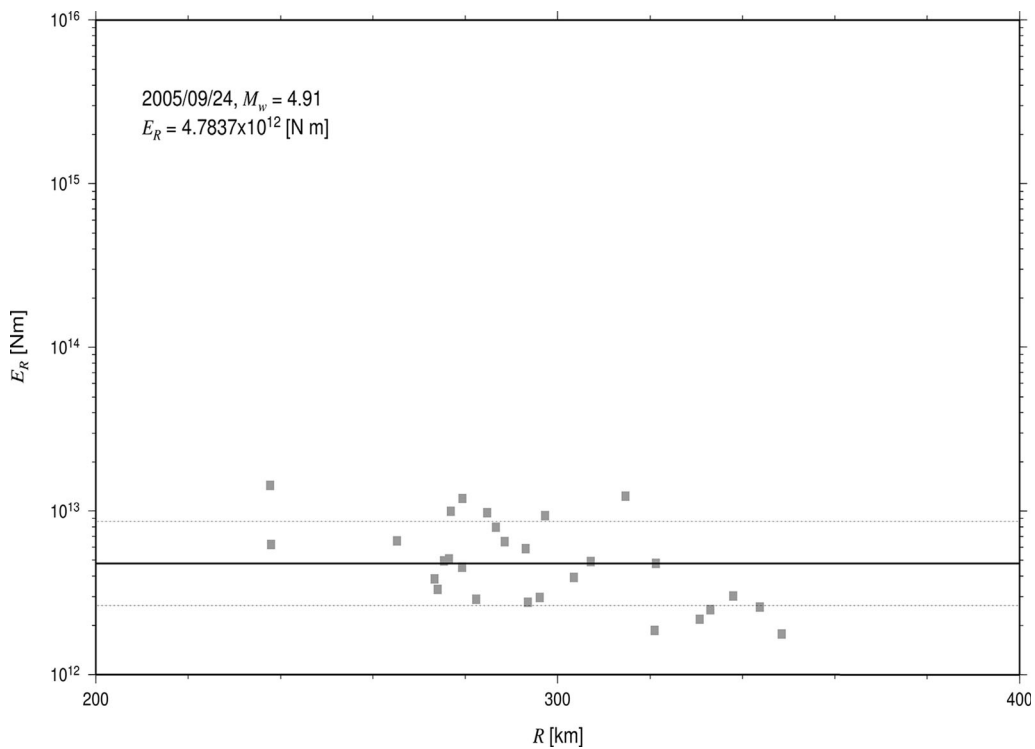


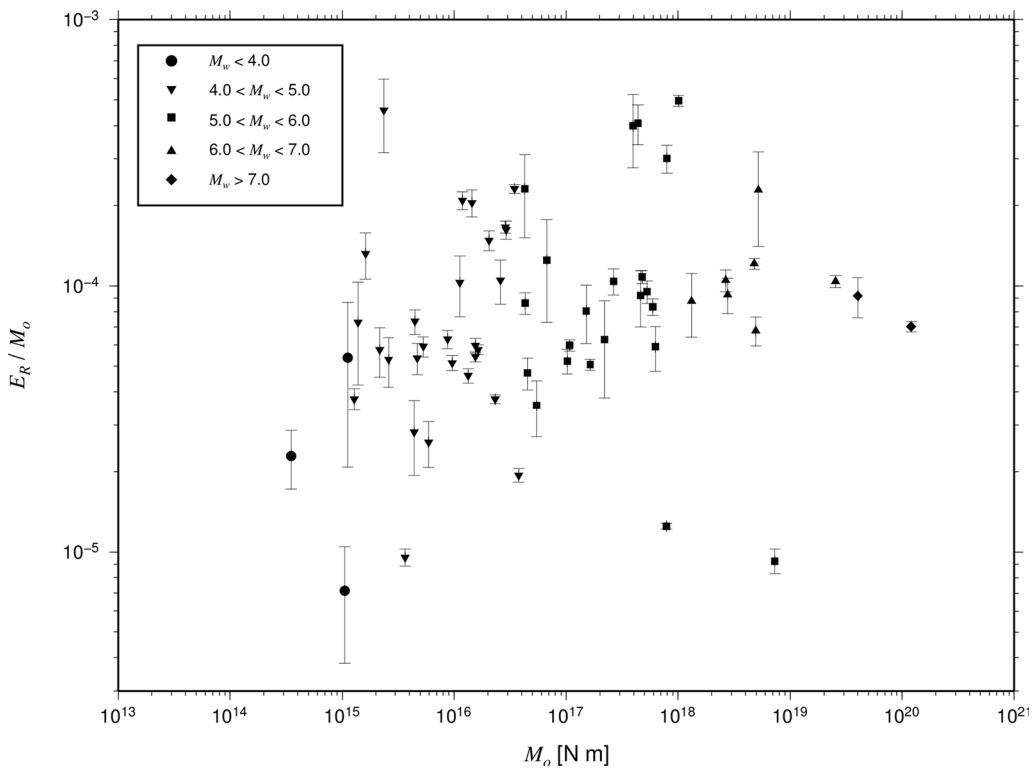
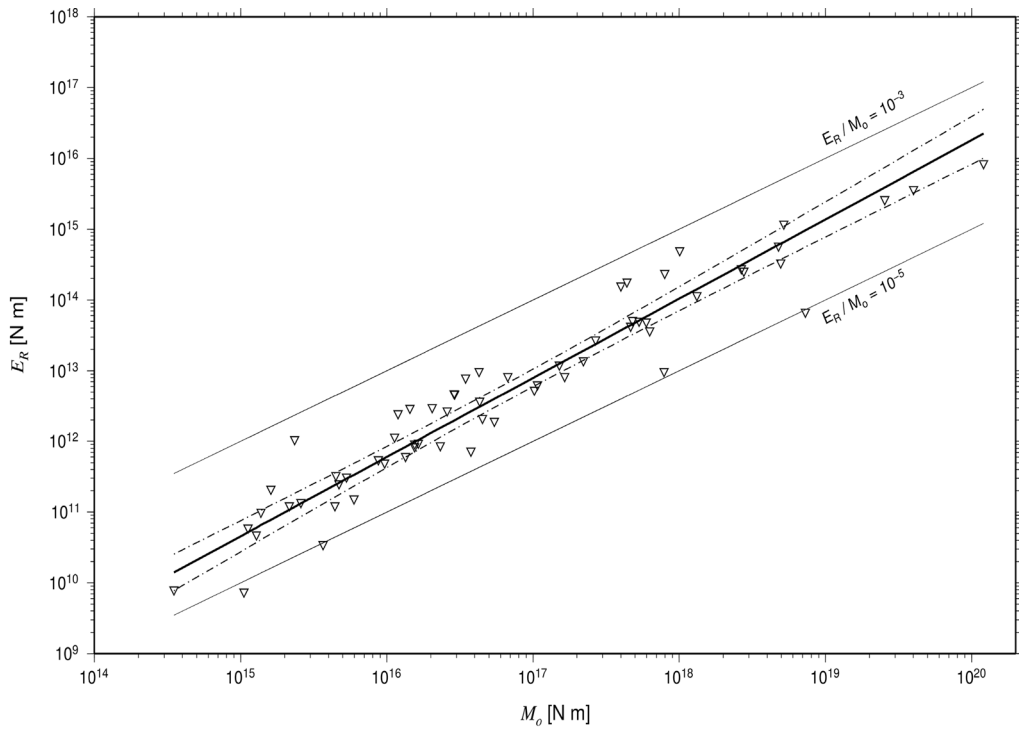
Figure 5
Example of radiated seismic energy estimated with regional data

at station i of event j under far-field point source approximation can be written as

$$A(f, R_{ij}) = CS(f)G(R_{ij})P(f)e^{-\pi f R_{ij}/\beta Q(f)}, \quad (2)$$

where

Figure 6
 E_R versus M_o for normal faulting inslab earthquakes (*upper panel*). The *solid black line* is the regression model. The *dashed lines* are the 95 % confidence intervals in the regression (*upper panel*). Comparison between E_R/M_o ratio and M_o with *error bars* for different magnitude intervals (*lower panel*)



$$C = \frac{R_{\theta\phi} F P (2\pi)^2}{4\pi\rho\beta^3}. \quad (3)$$

In these expressions, f is the frequency, R_{ij} is the hypocentral distance of the i th station with respect to j th event, $R_{\theta\phi}$ is the average radiation pattern (0.55; BOORE and BOATWRIGHT 1984), F is the free-surface amplification (2.0), P takes into account the partitioning of energy in the two horizontal components ($1/\sqrt{2}$), ρ and β are the density and shear velocity in the focal region, respectively, and $Q(f)$ is the quality factor, which includes both anelastic absorption and scattering. $S_j(f)$ is the source acceleration spectrum of event j , which may be written as

$$S_j(f) = f^2 \dot{M}_{oj}(f), \quad (4)$$

where $\dot{M}_{oj}(f)$ is the moment-rate spectrum. Following AKI (1967) and BRUNE (1970), the source spectrum $S(f)$ is given by

$$S_j(f) = \frac{f^2 \dot{M}_{oj}}{1 + \left(\frac{f}{f_c}\right)^2}, \quad (5)$$

where f_c is the corner frequency. Following BRUNE (1970) the corner frequency is given by the following equation:

$$f_{cj} = 4.91 \times 10^6 \beta \left(\frac{\Delta\sigma_j}{M_{oj}} \right)^{1/3}, \quad (6)$$

where $\Delta\sigma_j$ is the Brune stress drop in bars, β is in kilometers per second, and M_{oj} is the seismic moment in dyne centimeters. $P(f)$ is a high-cut filter defined by BOORE (1983) that fits well for frequencies greater than the cut-off frequency (f_{\max}). f_{\max} is an important parameter of earthquake engineering as it controls the peak ground acceleration. f_{\max} could be attributed to the source (e.g. PAPAGEORGIOU and AKI 1983a, b; YOKOI and IRIKURA 1991) or to the path and or recorded site effects (HANKS 1982; ANDERSON and HOUGH 1984). The form of the f_{\max} filter is defined as

$$P(f) = \left[1 + \left(\frac{f}{f_{\max}} \right)^{2s} \right]^{-1/2}, \quad (7)$$

where s controls the decay rate at high frequencies. In addition, we used the site correction described in the

Figure 7

Comparison between $\Delta\sigma$ and M_o (upper panel); $\Delta\sigma$ and depth (middle panel); η_R and M_o (lower panel), with error bars for different magnitude intervals

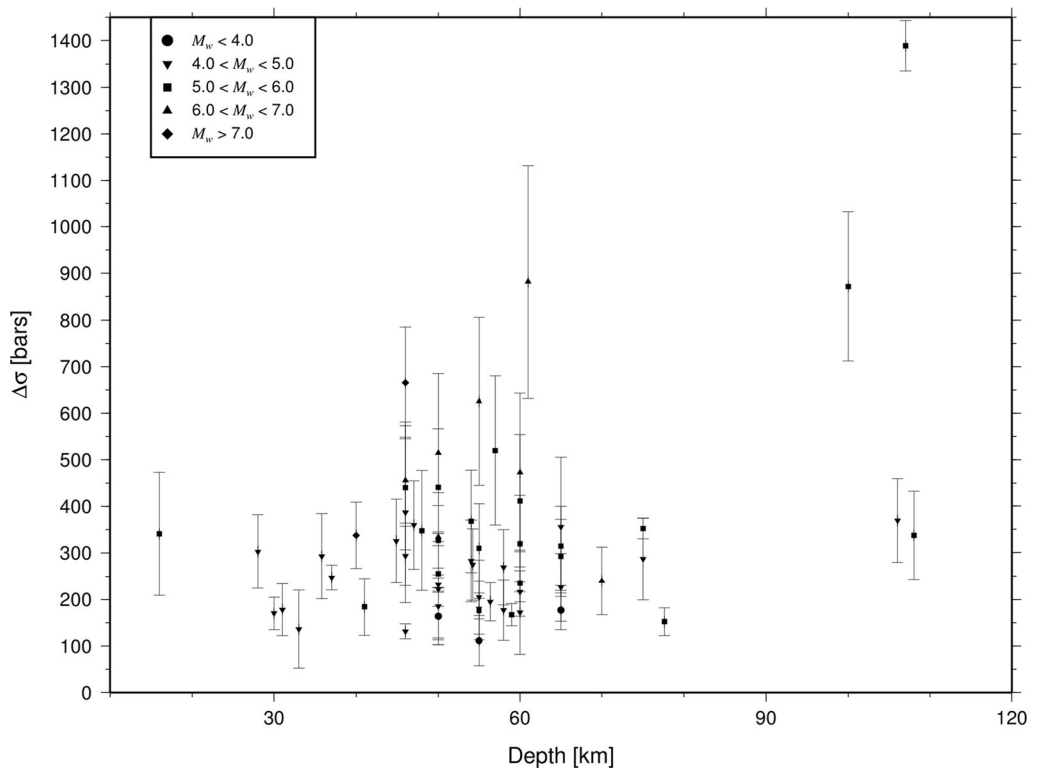
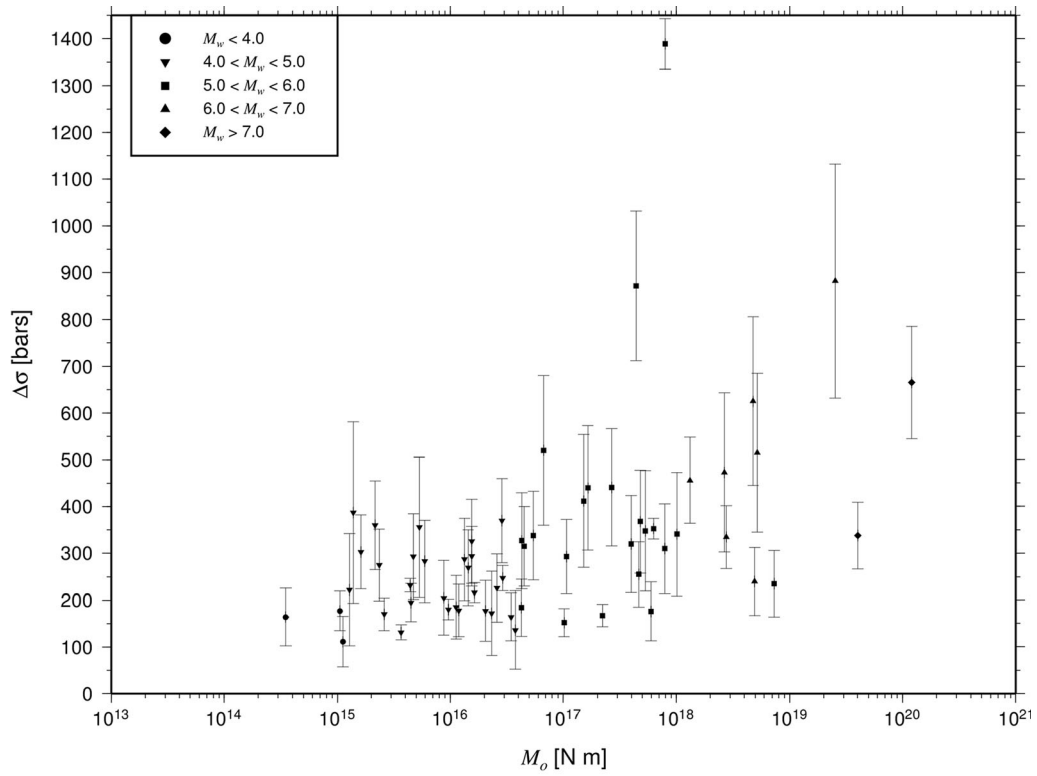
previous section, where the term $e^{-\pi\kappa f}$ is also known as the κ filter. Both filters can be combined in the source analysis (BOORE 2003). The source radius is estimated with the following expression: $r = 2.34\beta / 2\pi f_c$ based on BRUNE (1970). Average values $\langle \zeta \rangle$ were computed for each parameter (E_R , $\Delta\sigma$, f_c , f_{\max} , fault dimensions, and rupture area) (Table 3) following ARCHULETA *et al.* (1982) as

$$\langle \zeta \rangle = \text{anti log} \left\{ \frac{1}{N} \sum_{i=1}^N \log \zeta_i \right\}, \quad (8)$$

where N is the number of stations used. Equation (8) is used because in the case of simple arithmetic average, the mean values are biased towards the larger values. The corresponding standard deviation of the logarithm $SD(\log\langle \zeta \rangle)$ was also calculated from the relations of ARCHULETA *et al.* (1982) as

$$SD(\log\langle \zeta \rangle) = \left\{ \frac{1}{N-1} \sum_{i=1}^N [\log \zeta_i - \log\langle \zeta \rangle]^2 \right\}^{1/2}. \quad (9)$$

The source parameters are automatically estimated by fitting the acceleration spectra (Eq. 2) to observed spectra with different values of f_c , f_{\max} , and spectral flat level (Fig. 8). In this process, we minimize the root mean square error between the synthetic and observed spectra. The minimization is carried out using the matlab routine f_{\min} search. The selection of the appropriate time window is an important factor in estimating source parameters since it is affecting the seismic moment value. We used window lengths that include the maximum amplitude of the wave. Thus, the length of this time windows may be different for different events, depending on the magnitude of the earthquake and the hypocentral distance. Small events recorded at short distances tend to have shorter time-window lengths. By taking the shear-wave time window too short, the seismic moment will be underestimated. On the contrary, by taking the time window too long, the signal will be affected by coda waves. For this



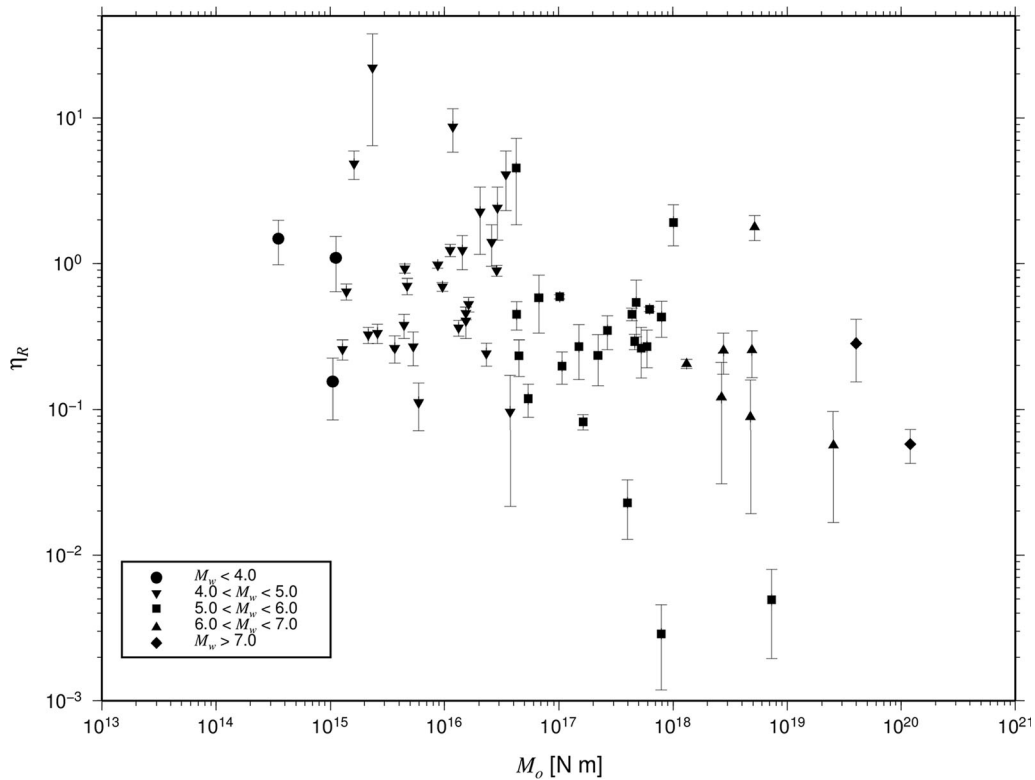


Figure 7
continued

reason, the S wave window starts from the S -phase onset and includes at least 85 % of the total energy of the recorded signal to provide stable source parameter estimates. This 85 % energy limit was proposed by some authors as the minimum bound for spectral decay parameters and attenuation analyses (e.g. CASTRO *et al.* 1996; FERNÁNDEZ *et al.* 2010). After testing different energy bands (from 85 to 95 %), we conducted our calculations considering a 95 % energy band. The window length was chosen such that it included the main S -wave arrival and 95 % of the total energy, starting at 3 % of the Fourier spectrum energy and ending at 98 % as recommended by several authors (CASTRO *et al.* 1990; ORDAZ and SINGH 1992; GARCÍA *et al.* 2009). Once we obtain a solution for each station, we use Eqs. 8 and 9 to estimate final parameters reported in Table 3.

3.4. Source Duration

Three measures of source duration of an earthquake have been reported in the literature: (1) total rupture duration (τ_t); (2) the pulse duration of each subevent (τ_p); and (3) the rise time (τ_r). In this study, we calculated τ_t and τ_p values for normal-faulting inslab events (Table 3). For complex events, we list the total duration as well as the pulse duration and the number of subevents (Table 3). On the other hand, for simple events, τ_t and τ_p are equal (Table 3). We performed a waveform inversion of near-source displacement records for some events to estimate the source duration, M_o , and focal mechanism following SINGH *et al.* (2000c). The inversion assumes that the events may be approximated by a point-source shear dislocation in an infinite space. This approximation is acceptable if the epicentral distance

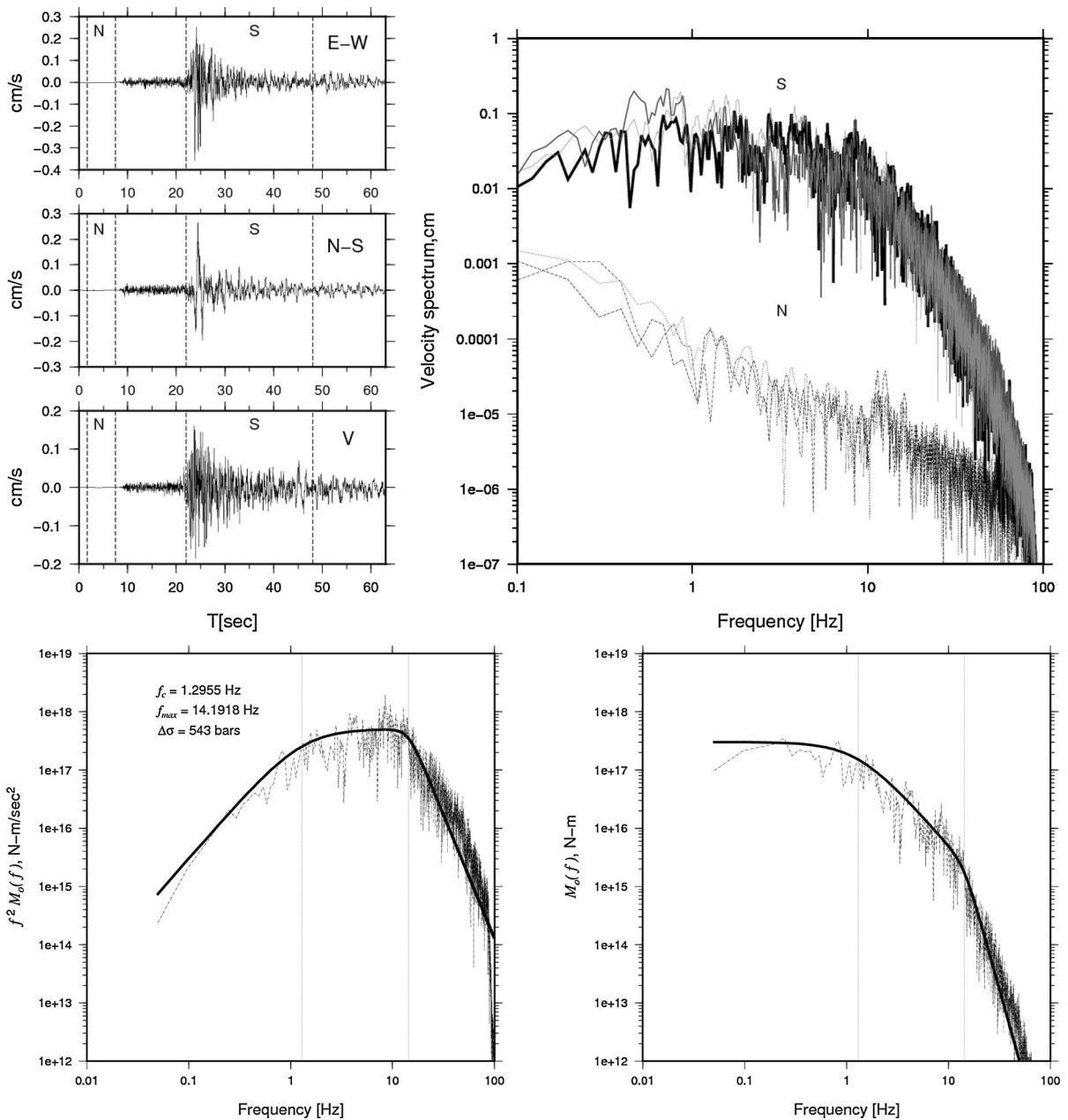
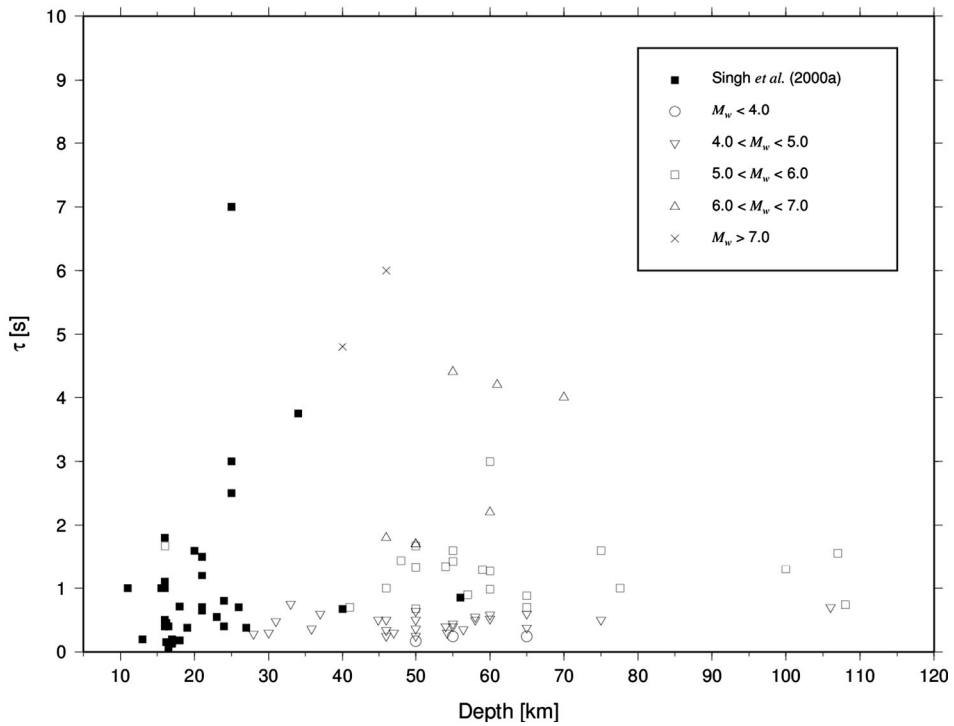
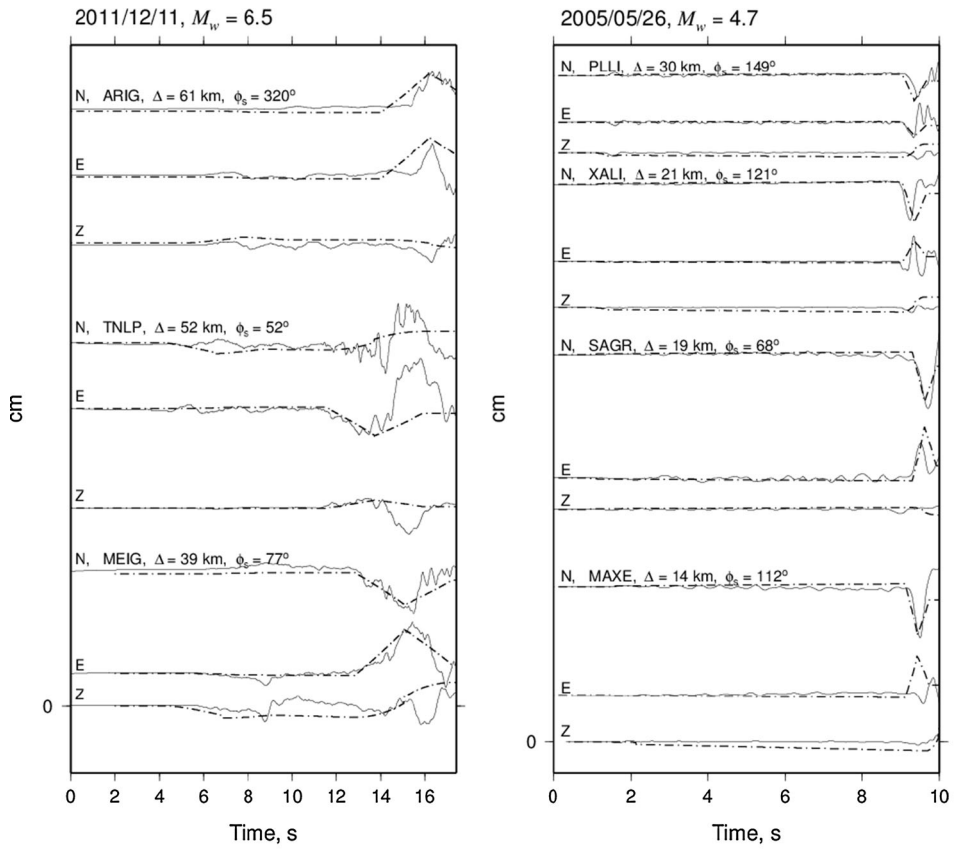


Figure 8

Example of the spectral analysis for event 52 (Tables 1, 3) ($M_w = 5.4$) recorded at station TNLP (Rock site, $R = 129$ km). Velocity traces with time windows of noise (N) and S-group waves (S) (upper left panels) and their spectra (upper right panel). Lower panels show the source acceleration and displacement spectra. Superimposed on the spectra are the predicted curves from an ω^2 source models (solid black curves)

is smaller than the depth. Synthetic seismograms include near-, intermediate-, and far-field terms (SINGH et al. 2000c). Theory predicts simple unipolar P and S displacement pulses. The effect of free

surface is approximately taken into account by multiplying the infinite-space synthetics by two (SINGH et al. 2000c). This approach has previously been used to estimate source parameters for normal-



◀Figure 9

Observed (continuous) and synthetic (*dashed*) displacement seismograms of events 32 and 56 (*upper panel*). The figure shows P and S waves recorded at the closest stations for these earthquakes. Synthetic displacements correspond to the focal mechanisms and seismic moments obtained in the inversion. Source duration plotted as a function of depth for the studied earthquakes for different magnitude ranges (*lower panel*). *Black squares* show source duration for interplate thrust earthquakes reported by SINGH *et al.* (2000a)

faulting inslab events (SINGH *et al.* 2007; PÉREZ-CAMPOS *et al.* 2010) and most commonly for shallow thrust interplate events in Mexico.

In the far-field, the body-wave displacement pulse is proportional to the source time function, on the assumption that the Q effect is negligible. Therefore, the source time function can directly be estimated from the displacement seismograms (SINGH *et al.* 2000c). P waves are a better choice to estimate source time functions due to the fact that P waves are less affected by attenuation than S waves (SINGH *et al.* 2000c). This requires that the area under the P pulse to be equal to M_0 (SINGH *et al.* 2000c). For this reason, whenever possible, P wave pulse is used to obtain source duration. The observed duration is a function of the takeoff angle of the ray and the azimuth of the recording station. The simplest waveform was taken to represent the shape of the source time function. In the case of several available recordings, an average value of the source duration is taken. For larger events ($M_w \geq 5$), we mainly estimated the source time function using the S pulse following SINGH *et al.* (2000c). Figure 9 shows an example of the estimation of duration of the events 34 and 56. The P and

the S waves recorded at the closest distances are shown in Fig. 9. The S waves show large variation, mostly because of contamination from P-wave coda. For these examples, we chose the station MEIG as the source time function with a duration of 4 s for event 56 (Fig. 9). For the event 34, we used the stations PLLL, MAXE, and SAGR as source time functions with an average duration of 0.4 s (Fig. 9). Table 3 shows the number of subevents (n), τ_p and τ_t . We also compared and model the source duration using the moment tensor inversion.

3.5. Regression Analysis

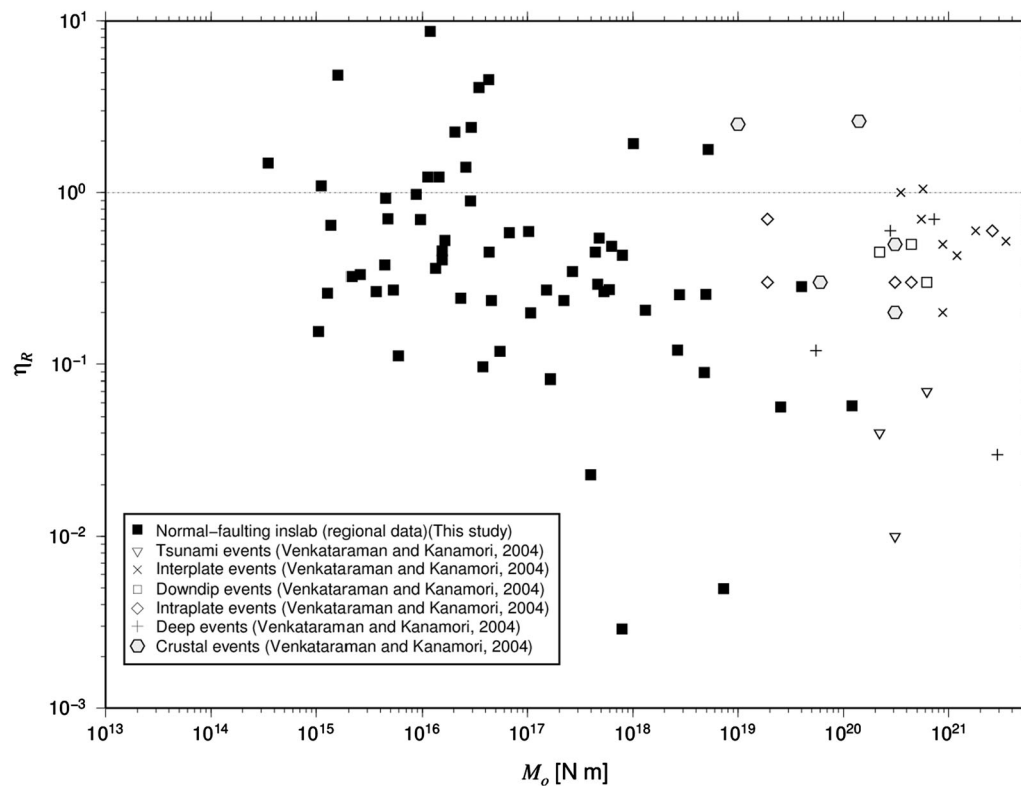
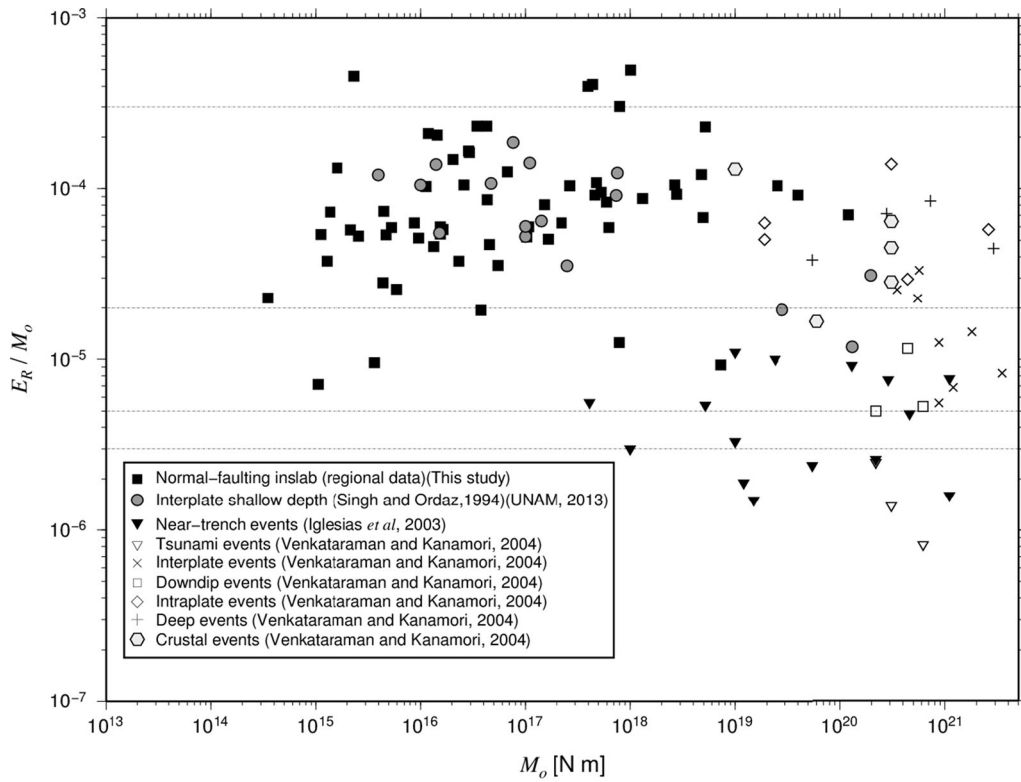
We derived scaling relationships for the source parameters described above (Table 4). Relationships between seismic moment and the source parameters are estimated using orthogonal least-squares regression analysis. Orthogonal regression minimizes the Euclidean distance to the regression line, instead of the vertical distance, and is, therefore, a better choice (BLASER *et al.* 2010). The resulting linear expressions are of the form: $\log(Y) = a + b M_0$, where Y is a seismic source parameter (Table 4). We calculate t statistics to evaluate the significance of each relationship, showing the 95 % confidence interval on the mean. The coefficient of determination R^2 defined as the square of the correlation coefficient takes values between 0 and 1, where values closer to 1 imply a better fit. This enables us to evaluate the correlation among various rupture parameters. Table 4 shows regression coefficients a and b , the standard errors sa , sb , standard deviation S_{xy} , as well as the coefficient of determination R^2 .

Table 4

Scaling coefficients between source parameters

$\log(Y) = a + b \log(X)$		b	sb	a	sa	S_{xy}	R^2
Y	X						
E_R	M_0	1.119	0.026	-6.128	0.440	0.257	0.958
r	M_0	0.241	0.010	-3.954	0.165	0.096	0.994
f_c	M_0	-0.214	0.010	4.221	0.166	0.096	0.994
f_{\max}	M_0	-0.090	0.005	2.545	0.090	0.052	0.998
τ_p	M_0	0.284	0.004	-4.892	0.076	0.045	0.984
τ_t	M_0	0.323	0.008	-5.514	0.128	0.076	0.966

M_0 and E_R in newton meter, r in kilometer, f_c and f_{\max} in hertz, τ_p and τ_t in seconds



◀Figure 10

Comparison between the obtained source parameters and other studies. The computed E_R/M_o ratios plotted as a function of seismic moment (*upper panel*). Symbols show different types of earthquakes and different studies as described in the legend. It is observed that tsunami and near-trench earthquakes have the smallest E_R/M_o ratios. Normal-faulting and interplate events based on regional data have the largest E_R/M_o ratios followed by the crustal and deep earthquakes estimated from teleseismic data. *Dashed lines* indicate the limits proposed by VENKATARAMAN and KANAMORI (2004) (see text). The computed η_R plotted as a function of seismic moment (*lower panel*). Symbols show different types of earthquakes and different studies as described in the legend. Most earthquakes have radiation efficiencies greater than 0.25

3.6. Stress Tensor Inversion

To study the stress field for normal-faulting inslab subduction zone events, we performed stress inversions of the obtained focal mechanisms applying an iterative joint inversion developed by VAVRYČUK (2014). We used this technique to determine the four parameters of the reduced stress tensor that models best the state of stress: the orientation of the three orthogonal principal stress axes σ_1 , σ_2 , and σ_3 (where $\sigma_1 \geq \sigma_2 \geq \sigma_3$) and the stress ratio $R = (\sigma_1 - \sigma_2) / (\sigma_1 - \sigma_3)$ (GEPHART and FORSYTH 1984). The iterative joint inversion provides an accurate value of shape ratio R for stress and fault orientations (VAVRYČUK 2014). In this method, a fault instability constraint is applied and the fault is identified with that nodal plane which is more unstable and thus more susceptible to faulting (VAVRYČUK 2014). Incorporating the fault instability constraint into the inversion leads to an iterative procedure. The uncertainties are calculated as the maximum differences between the results of the inversion for noise-free and noisy data with 1000 noise realizations (VAVRYČUK 2014). We also computed the maximum horizontal stress (SH_{\max}) with the formula of LUND and TOWNEND (2007).

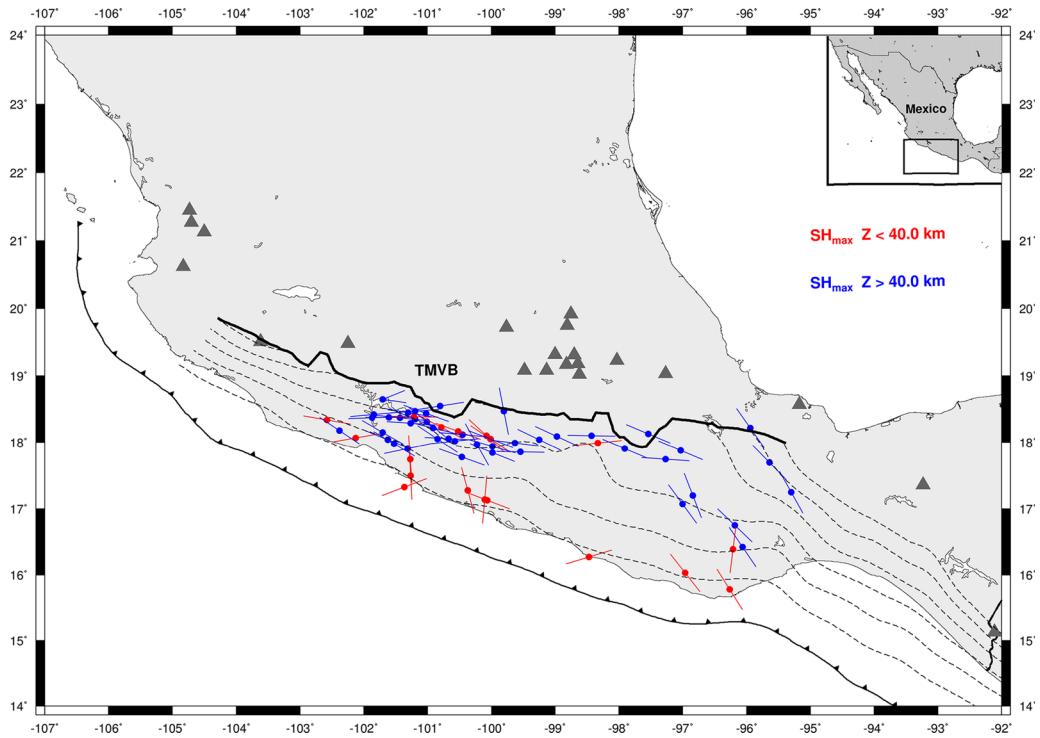
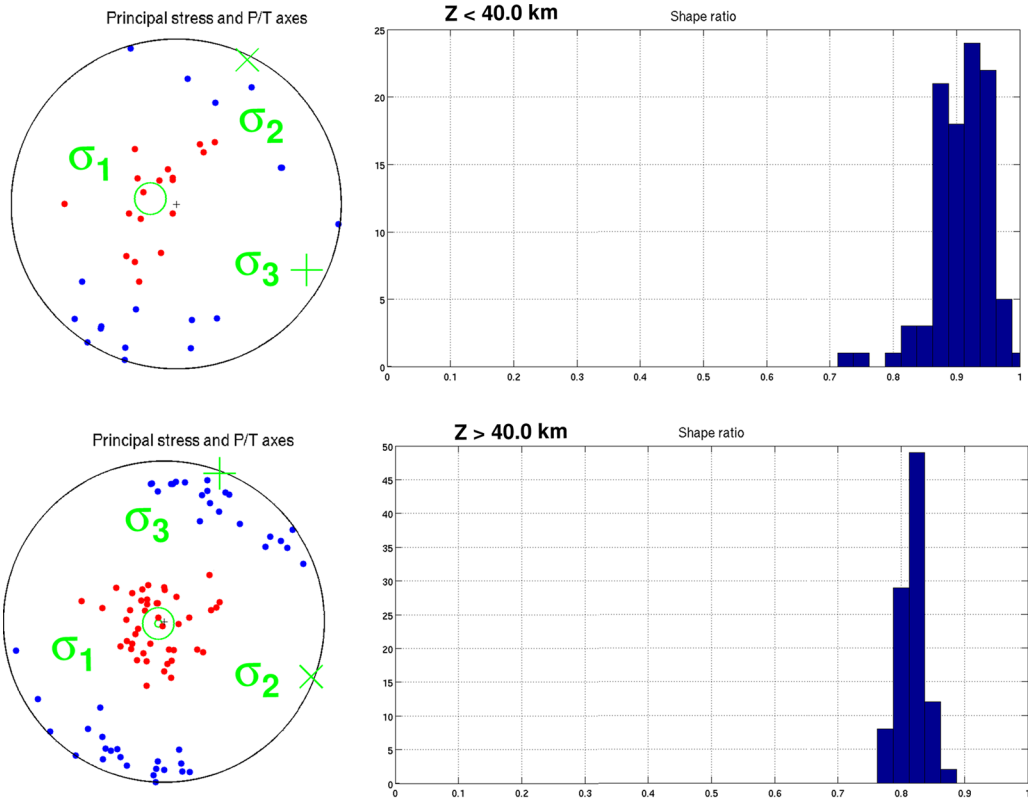
4. Results

The source parameters for 62 normal-faulting inslab events ($3.9 < M_w < 7.4$) have been estimated using different methods. The focal mechanisms and moment tensor solutions are consistent with previous studies and CMT solutions. Source parameter estimations are listed in Tables 1, 2, and 3. Table 4 shows the results from the regression analysis. All source

parameters have high determination coefficients ($R < 0.9$) and low standard deviations. Estimations of the E_R/M_o ratio range from 9.55×10^{-6} to 4.96×10^{-4} (Fig. 6). The results show that most of the E_R/M_o estimations are higher than 2×10^{-5} , thus similar to the values for interplate, crustal, and deep events (Fig. 10). The stress drop of the events varies from 111 to 1389 bars and shows large scatter (Table 3; Fig. 7). The results also show that there is no clear depth dependence of stress drop (Fig. 7). The seismic efficiency shows large scatter and ranges between 0.003 and 8.7, but most of the observations are in the ranges of 0.1–2.0 (Table 3; Fig. 7). Most of the obtained efficiencies have larger values than those reported for tsunami and very deep earthquakes by VENKATARAMAN and KANAMORI (2004) (Fig. 10).

The pulse duration of the events varies from 0.22 to 9 s and the number of subevents range from 1 to 3 (Table 3 and Fig. 12). The total duration varies from 0.22 to 14.5 s (Table 3). The results of SINGH et al. (2000a) showed also that there is no significant depth dependence for source duration (Fig. 12). The source duration results showed that near-source approach is in good agreement with moment tensor inversion results with careful selection of events and seismic stations. There is also no clear difference in terms of the source duration among the shallow thrust interplate and normal-faulting inslab events. The obtained scaling relations for τ_t and τ_p are similar to those obtained by SINGH et al. (2000a) (Fig. 12). The corner frequencies are in the range of 0.22–5.53 Hz (Table 3). f_{\max} varies from 5.5 to 16.82 Hz (Table 3). The results show a similar decreasing trend for both f_c and f_{\max} with increasing M_o (Fig. 13). The obtained scaling relationship between f_c and M_o differs slightly from the model of García et al. (2004). The standard deviation values for f_c and M_o (in spectral analysis and moment tensor inversion) with the majority of being less than 1 Hz and 0.50 Nm, respectively, confirm the accuracy of derived source parameters such as the source dimensions and stress drop. The source dimensions in terms of the radius of the circular fault vary from about 0.35 to 8.46 km (Table 3). The source area ranged from 0.5 to 230 km² (Table 3). Both r and A show a linear scaling with M_o (Fig. 14).

The results from stress tensor inversion are shown in Fig. 11 and Table 5. Results show that the



◀Figure 11

Results of stress tensor inversion for shallow ($Z < 40$ km; $N = 18$) and intermediate-depth ($Z > 40$ km; $N = 44$) earthquakes, respectively (*upper panel*). Circles represent the maximum principal stress (σ_1), crosses represent the intermediate principal stress (σ_2), and plus markers represent the minimum principal stress (σ_3) (*upper panel*). The right part of the upper panels shows histograms of R values versus frequency. The orientation of maximum horizontal compressional axes (SH_{\max}) versus depth (*middle panel*). Orientation of tensional axes for shallow and intermediate-depth events, respectively (*lower panel*)

maximum principal compressional stress (σ_1) strikes 282° with a plunge of 76.8° , the intermediate principle compressional stress (σ_2) strikes 26.1° with a plunge of 3.2° , and the minimum principal compressional stress (σ_3) strikes 116.9° with a plunge of 12.8° for shallow events ($Z < 40$ km). For the case of intermediate-depth events ($Z > 40$ km), the results show that the maximum principal compressional stress (σ_1) strikes 253° with a plunge of 87° , the intermediate principle compressional stress (σ_2) strikes 110.5° with a plunge of 2.4° , and the

minimum principal compressional stress (σ_3) strikes 20.4° with a plunge of 1.8° . The distribution of the relative stress magnitude (R), resulting from the iterative bootstrap analysis is shown by the histograms in Fig. 11. The stress ratios R of 0.82 and 0.91 (for shallow and intermediate-depth events, respectively), indicate that $\sigma_2 \approx \sigma_3$. The slight difference is apparent in the plunges of σ_1 and σ_2 ($\leq 15^\circ$) (Table 5). The results show that the tensional axes are parallel to the dip direction of the subducted plate (Fig. 11). At depths greater than 40 km, the maximum horizontal stresses are oblique to the dip direction following the general trend of the slab geometry (Fig. 11).

5. Discussion

Intermediate-depth earthquakes occur at depths where temperatures and pressures exceed those at which brittle failure is expected (at depths of

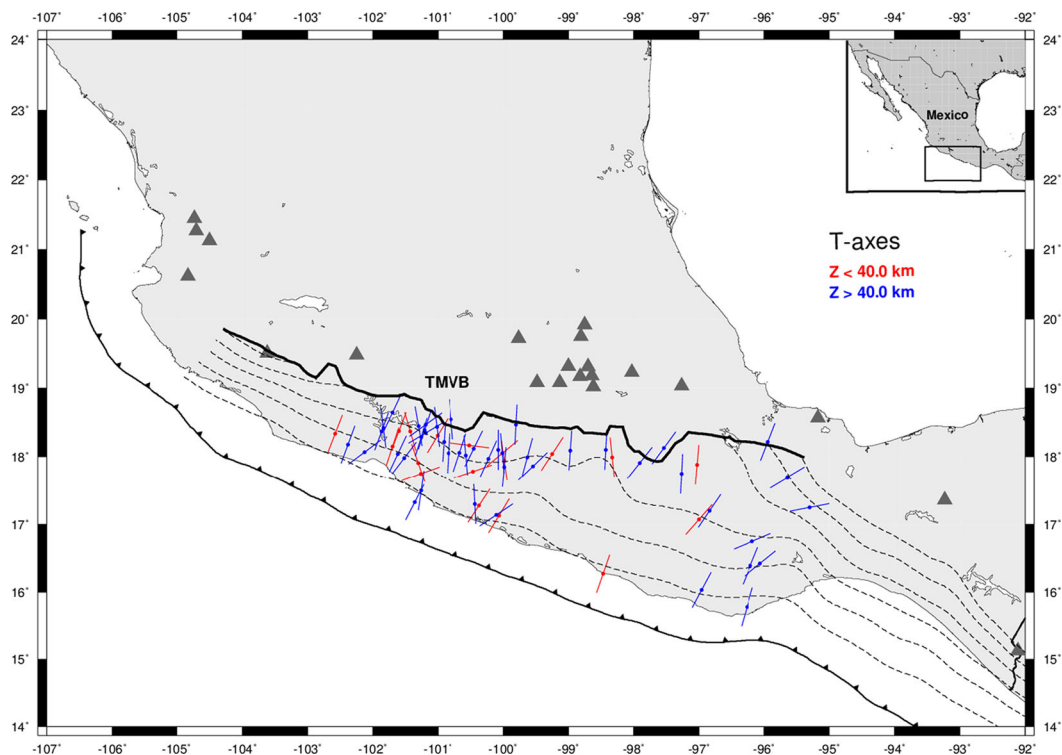


Figure 11
continued

Table 5
Stress tensor results

σ_1 Azimuth/plunge	σ_2 Azimuth/plunge	σ_3 Azimuth/plunge	SH _{max}	R	Depth
282.0°/76.8°	26.1°/3.2°	116.9°/12.8°	60.80	0.91	Z < 40 km
253.0°/87.0°	110.5°/2.4°	20.4°/1.8°	10.90	0.82	Z > 40 km

Stress ratio is defined by $R = (\sigma_1 - \sigma_2)/(\sigma_1 - \sigma_3)$

50–300 km) (FROHLICH 2006). The physical mechanism remains unclear because ambient temperatures and pressures are expected to lead to ductile, rather than brittle deformation (GREEN and HOUSTON 1995; FROHLICH 2006). Some authors suggest that the dehydration embrittlement can be a possible mechanism (GREEN and HOUSTON 1995; FROHLICH 2006; HOUSTON 2007), which posits that earthquakes are triggered by the release of fluids during metamorphic dehydration reactions, raising the pore pressure and permitting brittle failure. Some studies provide evidence that intermediate-depth earthquakes have high stress drop and low radiation efficiency ($1 < \Delta\sigma < 100$ MPa; $\eta_R = 0.022$ for Bucaramanga Colombia, PRIETO et al. 2013; and $110 < \Delta\sigma < 280$ MPa $\eta_R = 0.04$ – 0.1 for Bolivia, KANAMORI et al. 1998; and VENKATARAMAN and KANAMORI 2004; among others). Our estimates of η_R are in the range of 0.1–1.0, for most of the events, but the results show also large scatter (Fig. 7). In a few cases $\eta_R > 1$, which implies that estimates of E_R and/or $\Delta\sigma$ are inaccurate, or the model we use to calculate η_R is inappropriate (VENKATARAMAN and KANAMORI 2004). By comparing our estimates of η_R with results of other tectonic environments, we observe that η_R is higher than values for tsunami and very deep earthquakes (Fig. 10). This suggests that intermediate-depth normal-faulting earthquakes dissipate less energy than deep and near-trench events (Fig. 10).

Many authors have suggested that the stress drop is roughly independent of the seismic moment with typical values ranging from 0.1 to 100 MPa for different data sets (KANAMORI and ANDERSON 1975; ABERCROMBIE 1995; among others). Potential causes for a wide variation of $\Delta\sigma$ between different data sets include difference in tectonic settings, the amount of water present, variations in rupture velocity, and variations in fault plane normal stress (TOMIC et al.

2009). Intermediate-depth and deep earthquakes have higher stress drop (GARCÍA et al. 2004 for the Mexican case). Our stress drop estimates are in agreement with previous studies in Central Mexico for normal-faulting inslab events (SINGH et al. 1999, 2000b, 2014; GARCÍA et al. 2004; SINGH et al. 2007; PÉREZ-CAMPOS et al. 2010; SINGH et al.). Our results show no trend between stress drop and seismic moment (Fig. 7). We noted that the stress drop is highly variable at intermediate depth (Fig. 7). The stress drop variation can also be related to uncertainties in the corner frequency estimates. We analyzed the variation of estimated corner frequencies for different time window lengths (expressed in terms of energy percentage). We observed that the 95 % energy band provides stable earthquake source parameter estimates. We also used the criteria proposed by HAVSKOV and OTTEMÖLLER (2010) to assess if the obtained corner frequencies are “reasonable”. This criterion is based on a scaling relationship for f_c as function of M_w , $\Delta\sigma$, and β . Our estimates of corner frequencies can be considered as reliable and stable. For our stress drop estimates, an average uncertainty of 27 % can be expected, but it can fluctuate up to 60 % for some individual station estimates of stress drop. Similar results were reported by KANE et al. (2011) (a minimum uncertainty level of 30 %).

There is an ongoing debate whether the E_R/M_0 ratio and thus the apparent stress (σ_a) (the E_R/M_0 ratio scaled by the rigidity coefficient) is constant over some magnitude range. Many studies found that σ_a and thus E_R/M_0 increase with seismic moment (SINGH and ORDAZ 1994; ABERCROMBIE 1995; MAYEDA and WALTER 1996; PÉREZ-CAMPOS and BEROZA 2001). On the other hand, many other seismological observations are not consistent with σ_a and E_R/M_0 increasing with seismic moment (MCGARR 1999; IDE and BEROZA 2001; IDE et al. 2003; YAMADA et al. 2005) based on

data in the magnitude range of $-1 < M_w < 7$. Our results support the hypothesis that the E_R/M_o ratio is independent of the event size (Figs. 7, 10). We compared our results with those obtained from different types of earthquakes. We observed that intermediate-depth normal-faulting inslab events have higher E_R/M_o ratios than near-trench and tsunami earthquakes, but similar to interplate, crustal, and deep events (Fig. 10).

By comparing our results with previous studies, we observe that E_R/M_o ratios estimated from regional data are higher than reported values for interplate and downdip events derived from teleseismic data (Fig. 10). This highlights the issue that estimations of the E_R/M_o ratio present large scatter due to difficulties in calculating M_o and/or E_R . For example, estimates of seismic moment for a specific event may vary by a factor of two (± 0.2 in M_w) between stations (PRIETO et al. 2004) and estimates of radiated seismic energy by a factor of 5–10 (e.g., SINGH and ORDAZ 1994). M_o is estimated from the rather well-constrained low-frequency part of the earthquake spectrum as opposed to E_R . Radiated energy, estimated from the high-frequency part of the spectrum is strongly affected by attenuation of seismic waves and limited bandwidth of the recording instruments, which also affect estimates of corner frequencies. A more accurate approach to estimate source parameters is the Empirical Green's function (EGF) technique. In this technique, path and site effects are removed by spectral division between a main event and an earthquake with the following characteristics (known as EGF): (1) The location of the event lies on the mainshock fault; (2) the focal mechanism must be similar; and (3) the aftershock should be one or two magnitudes smaller than the mainshock. For most of the intermediate depth earthquakes, finding an appropriate EGF was difficult and, therefore, we could not apply this technique.

The results for source duration over the entire depth range showed no clear evidence that the duration of deep events is significantly different from that of shallow ones. Similar results were found by SINGH et al. (2000a) based on shallow thrust interplate and a few intermediate-depth normal-faulting events in Central Mexico. The obtained scaling relationships are similar to the models obtained by SINGH et al. (2000a) for τ_t and

τ_p (Fig. 12). This could be the product of the applied techniques and/or the tectonic environment. Our models for τ_t and τ_p are very similar because of the limited number of events with $M_w > 6.5$. By comparing our source duration relationships with models derived from teleseismic data in a similar magnitude range, we observed an overestimation of the source duration. This overestimation may be associated with inherent characteristics of the methods used. In our analysis, we combined two methods to estimate seismic source duration. The first one is based on a simple inversion scheme to retrieve source parameters of earthquakes recorded at close distances. This method assumes that the events may be approximated by a point-source. This method is only acceptable if the epicentral distance, is smaller than the earthquake depth, so the method is not suitable for all the studied events. The second approach that we used to estimate source duration is the moment tensor inversion. In this case, source duration estimates depend on the accuracy to generate synthetic seismograms. According to YAGI and FUKAHATA (2011), the Green's functions can be a major source of error in the inversions. Our results showed that both approaches are in good agreement. The differences also arise from the fact that in many studies the reported duration refers to total rupture duration (often with several subevents), specially for large events.

The obtained scaling relations for f_c and f_{max} showed similar scatter patterns and linear trends with M_o (Fig. 13). The observed values of f_{max} agree well with worldwide observations. The obtained scaling relationship between f_c and M_o is in good agreement with the model obtained by GARCÍA et al. (2004) derived with the same earthquake source model (Fig. 13). The differences may be related to the number of events analyzed and the magnitude range used (62 events with $3.9 < M_w < 7.4$ for this study and 17 events with $4.1 < M_w < 7.4$ for GARCÍA et al. 2004). The determination of the corner frequency is not straightforward as it depends on the transition between the low- and high-frequency fall of rate. This directly affects the estimation of source dimensions, and thus the stress drop. The standard deviation value for f_c with the majority of the observations is less than 0.31 Hz, confirming the accuracy of derived source parameters such as the source dimensions and stress

drop. For all the events, the source radius and area correlate well with seismic moment (Fig. 14). Estimation of accurate hypocentral parameters and focal mechanism can provide important information about the slip, fault structure at depth, and the stress field in seismically active areas. Our focal mechanism solutions results are in agreement with the tectonics of the subducted slab in Central Mexico. The moment tensor solutions are consistent with those of previous studies and the differences can be associated with the velocity structure and the method used to calculate the Green's functions. Most of the results of this study are based on the modeling of displacement and velocity spectra which requires several assumptions and applied corrections. Uncertainties in the estimated source parameters and data scatter in the scaling laws may reflect site effects that are not taken into account.

PACHECO and SINGH (2010) classified inslab earthquakes in Mexico into three different groups: (1) events that exhibit downdip tension; (2) events that reveal downdip compression; and (3) events with unusual strike-slip or normal fault mechanism with strike oriented at an oblique angle to the trench. Our results for stress inversion showed that the tensional axes are orientated in a direction parallel to the gradient of subducted oceanic plate (Fig. 11). These results are in agreement with previous stress studies (PARDO and SUÁREZ 1995; BRAVO et al. 2004; PACHECO and SINGH 2010). We observed complex stress distribution between 100 and 102°W at shallow depths ($Z < 40$ km). According to PARDO and SUÁREZ (1995), this complex stress pattern may be related with a rapid change in dip. On the other hand, the orientation of SH_{\max} for shallow events may be associated with slab bending upward to become subhorizontal (PARDO and SUÁREZ 1995). The heterogeneity in the regional stress field may be related with the simultaneous occurrence of group 1 and 3 events at shallow depths. PACHECO and SINGH (2010) suggested that group 3 earthquakes may represent localized stress concentrations due to contortions in the subducted plate or reactivation of old transform faults (PACHECO and SINGH 2010). Overall, the source parameter estimates are robust and reliable. Source parameters and stress state are consistent with the subduction zone system studies.

6. Conclusions

Earthquake source parameters' behavior for normal-faulting inslab earthquakes in Central Mexico are in agreement with other source parameter studies at subduction zones. The highest E_R , E_R/M_o , and $\Delta\sigma$ are associated with normal-faulting inslab events. This may be explained by the mechanism dependence of E_R reported in previous studies. The E_R/M_o ratio and $\Delta\sigma$ show no trend with seismic moment. Stress drop suggests an overall increment with source depth, albeit with the large scatter characteristic of stress drop measurements. The radiated efficiencies have similar values to those obtained from interplate events, but higher than near-trench events. The examination of the data over the entire depth range shows no clear evidence that the duration of deep earthquakes is significantly different from that of shallow ones. The uncertainty quantification shows that the source parameters and thus the scaling relationships are robust. Therefore, reliable source parameter estimations can be carried out using these relationships. The stress inversion results show heterogeneity in the stress field and variability with depth.

Acknowledgments

This research was funded by the Mexican National Council for Science and Technology (CONACYT) (Postdoctoral scholarship 170162/2014 and Catedras program-project 1126). We also thank the Incorporated Research Institutions for Seismology (IRIS) for providing us with data of the MASE, VEOX, CODEX and MARS arrays. The authors would like to thank the Mexican National Seismological Service (SSN) at UNAM for providing the data of the broadband seismometer network. Strong ground motion records were obtained from the Mexican strong ground motion database from stations operated by the National Center for Disaster Prevention (CENAPRED); the Geophysics and Engineering Institutes at UNAM. Leonardo Ramírez-Guzmán and Citlali Pérez-Yáñez kindly provided us with some of the strong-motion records analyzed in this study.

Appendix

Comparison of the obtained scaling relationships with other models. See Figs. 12, 13 and 14.

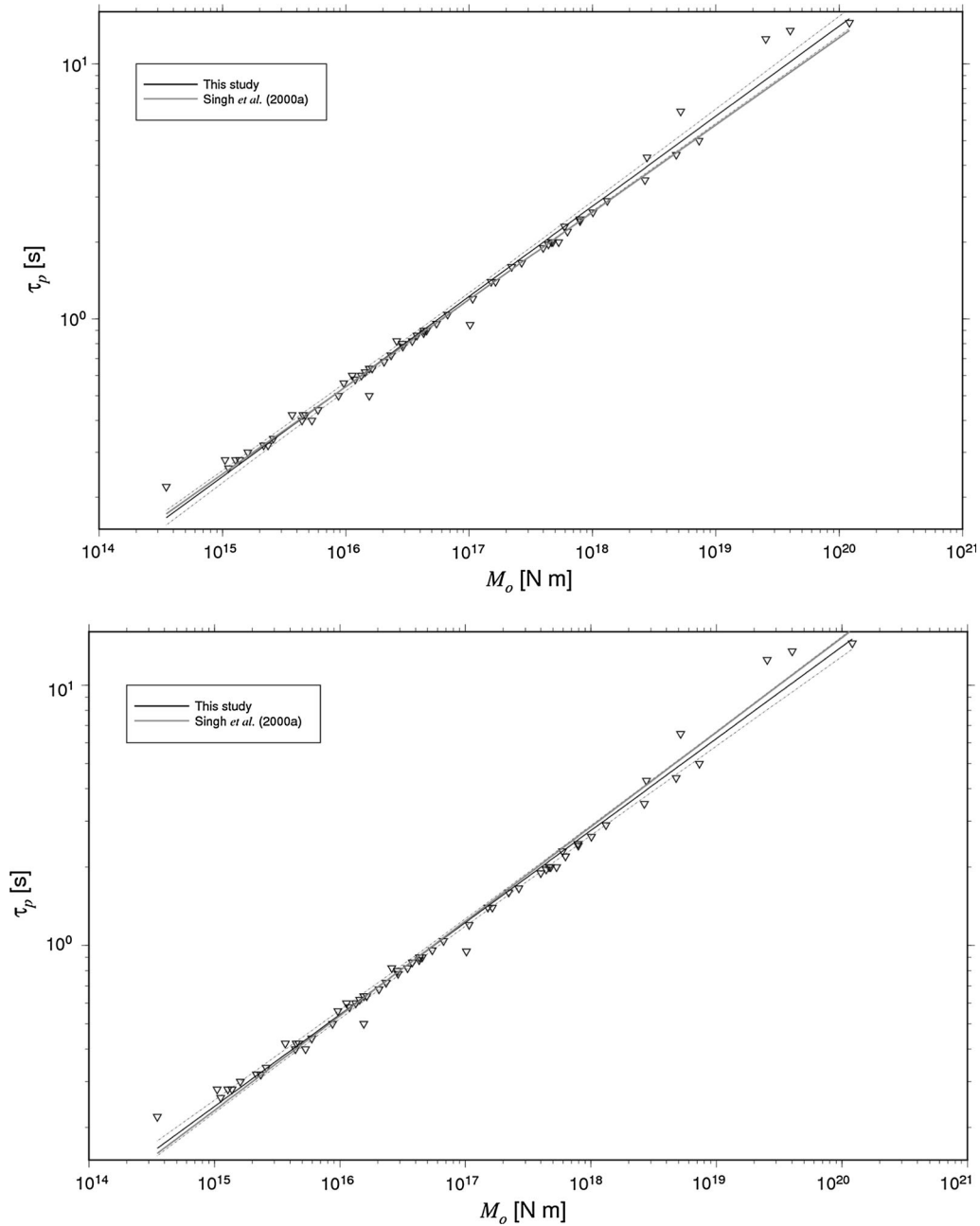


Figure 12

Relation between seismic moment and source duration from this study (black lines) and the study of SINGH *et al.* (2000a) (gray lines). The upper panel shows the pulse duration, while lower panel shows the total duration

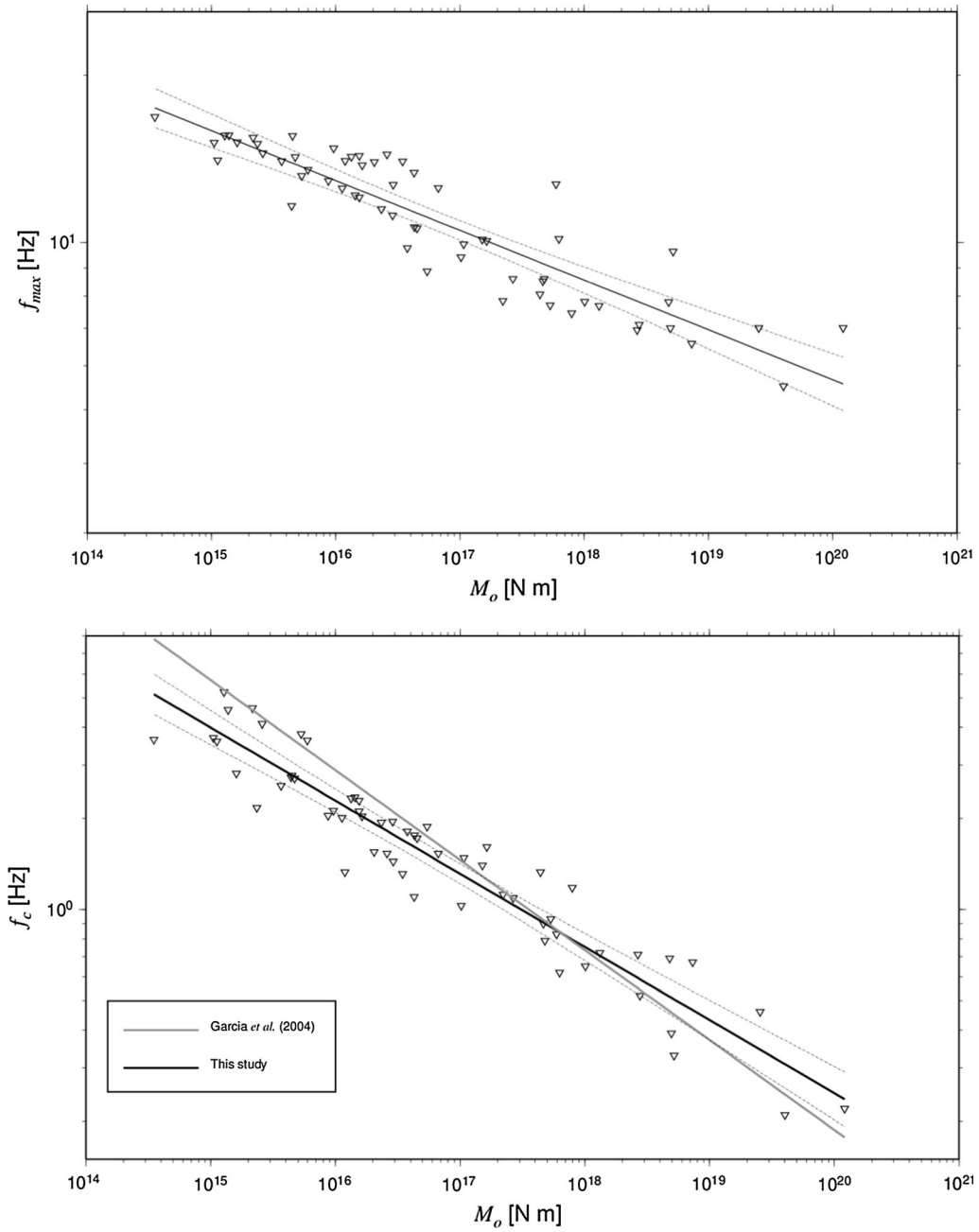


Figure 13

Scaling relationships for f_{max} (upper panel) and f_c (lower panel) (black lines). The dashed lines are the 95 % confidence intervals in the regressions. In the lower panel, the gray line shows the model of GARCÍA *et al.* (2004)

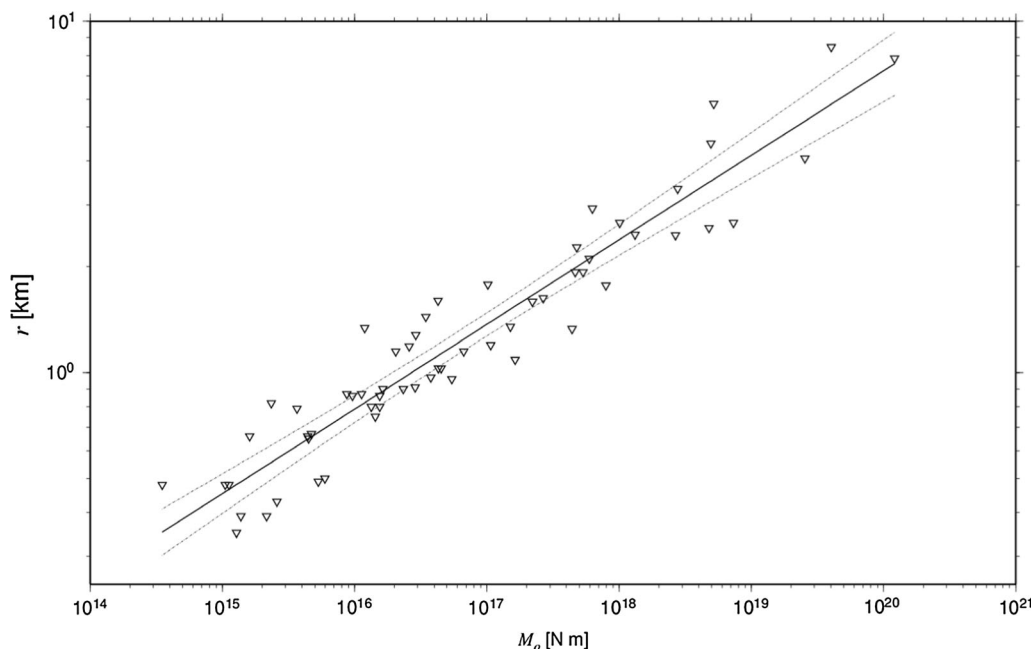


Figure 14

Scaling relationships for the source radii. The solid black lines are the regression models. The dashed lines are the 95 % confidence intervals in the regressions

REFERENCES

- ABERCROMBIE, R.E. (1995), *Earthquake source scaling relationships from -1 to $5 M_L$ using seismograms recorded at 2.5 km depth*, J. Geophys. Res. *100*, 24015–24036.
- AKI, K. (1967), *Scaling law of seismic spectrum*, J. Geophys. Res. *72*, 1217–1231.
- ANDERSON, J.G., and HOUGH, S.E. (1984), *A model for the shape of the Fourier amplitude spectrum of acceleration at high frequencies*, Bull. Seism. Soc. Am. *74*, 1969–1993.
- ARCHULETA, R.J., E. CRANSWINCK, E., MUELLER, CH., and SPUDICH, P. (1982), *Source parameters of the 1980 Mammoth lakes, California, earthquakes sequence*, J. Geophys. Res. *87*, 4595–4607.
- BALTAY, A., PRIETO, G., and BEROZA, G.C. (2010), *Radiated seismic energy from coda measurements and no scaling in apparent stress with seismic moment*, J. Geophys. Res. *115*, B08314. doi:10.1029/2009JB006736.
- BLASER, L., KRÜGER, F., OHRNBERGER, M., and SCHERBAUM, F. (2010), *Scaling relations of earthquake source parameter estimates with special focus on subduction environment*, Bull. Seism. Soc. Am. *100*, 2914–2926.
- BOORE, D.M. (1983), *Stochastic simulation of high-frequency ground motions based on seismological generic rock site models of the radiated spectra*, Bull. Seism. Soc. Am. *73*, 1865–1894.
- BOORE, D.M., and BOATWRIGHT, J.L. (1984), *Average body-wave radiation coefficient*, Bull. Seism. Soc. Am. *74*, 1615–1621.
- BOORE, D.M., JOYNER, W.B., (1997), *Site amplifications for generic rock sites*, Bull. Seismol. Soc. Am. *87*, 327–341.
- BOORE, D.M. (2003), *Simulation of ground motion using the stochastic method*, Pure Appl. Geophys. *160*, 635–676.
- BOS, A.G., NOLET, G., RUBIN, A., HOUSTON, H., and VIDALE, J.E. (1998), *Duration of deep earthquakes determined by stacking global seismograph network seismograms*, J. Geophys. Res. *103*, 21059–21065.
- BRAVO, H., REBOLLAR, C.J., URIBE, A., and JIMENEZ, O. (2004), *Geometry and state of stress of the Wadati-Benioff zone in the Gulf of Tehuantepec, Mexico*, J. Geophys. Res. *109*, B04307. doi:10.1029/2003JB002854
- BRUNE, J.N. (1970), *Tectonic stress and the spectra of seismic shear waves from earthquakes*, J. Geophys. Res. *75*, 4997–5009.
- CASTRO, R.R., ANDERSON, J.G., and SINGH, S.K. (1990), *Site response, at attenuation, and source spectra of S waves along the Guerrero, Mexico subduction zone*, Bull. Seism. Soc. Am. *80*, 1481–1503.
- CASTRO, R.R., PACOR, F., SALA, A., PETRUNGARO, C. (1996), *S wave attenuation and site effects in the region of Friuli, Italy*, J. Geophys. Res. *101*, 22355–22369.
- CAMPILLO, M., SINGH, S.K., SHAPIRO, N., PACHECO, J.F., and HERMANN, R.B. (1996), *Crustal structure of the Mexican volcanic belt, based on group velocity dispersion*, Geofisica Int. *35*, 361–370.
- CHOY, G.L., and BOATWRIGHT, J.L. (1995), *Global patterns of radiated seismic energy and apparent stress*, J. Geophys. Res. *100*, 18205–18228.
- CHOY, G.L., and KIRBY, S.H. (2004), *Apparent stress, fault maturity and seismic hazard for normal-fault earthquakes at subduction*

- zones, *Geophys. J. Int.* 159, 991–1012. doi:10.1111/j.1365-246X.2004.02449.x
- COCCO, M., PACHECO, J., SINGH, S.K., and COURBOULEX, F. (1997), *The Zihuatanejo, Mexico, earthquake of 1994 December 10 (M = 6.6): source characteristics and tectonic implications*, *Geophys. J. Int.* 131, 135–145.
- FERNÁNDEZ, A.I., CASTRO, R.R., and HUERTA, C.I. (2010), *The spectral decay parameter kappa in Northeastern Sonora, Mexico*, *Bull. Seism. Soc. Am.* 100, 196–206.
- FROHLICH, C. (2006), *Deep earthquakes*, Cambridge Univ. Press, Cambridge.
- GARCÍA, D., SINGH, S.K., HERRÁIZ, M., PACHECO, J.F., and ORDAZ, M. (2004), *Inslab earthquakes of Central Mexico: Q, source spectra, and stress drop*, *Bull. Seism. Soc. Am.* 94, 789–802.
- GARCÍA, D., SINGH, S.K., HERRÁIZ, M., ORDAZ, M., and PACHECO, J.F. (2005), *Inslab earthquakes of Central Mexico: peak ground-motion parameters and response spectra*, *Bull. Seism. Soc. Am.* 95, 2272–2282.
- GARCÍA, D., SINGH, S.K., HERRÁIZ, M., ORDAZ, M., PACHECO, J.F., and CRUZ-JIMÉNEZ, H. (2009), *Influence of subduction zone structure on coastal and inland attenuation in Mexico*, *Geophys. J. Int.* 179, 215–230.
- GEPHART, J.W., and FORSYTH, D.W. (1984), *An improved method for determining the regional stress tensor using earthquake focal mechanism data: application to the San Fernando earthquake sequence*, *J. Geophys. Res.* 89, 9305–9320.
- GREEN, H.W., and HOUSTON, H. (1995), *The mechanics of deep earthquakes*, *Annu. Rev. Earth Planet. Sci.* 23, 169–213.
- HANKS, T. C. (1982), f_{max} , *Bull. Seism. Soc. Am.* 72, 1867–1879.
- HERRMANN, R.B., and HUTCHENSEN, K. (1993), *Quantification of m_{LG} for small explosions*, in Report PL-TR-93-2070, 90 pp., Phillips Laboratory, Hanscom Air Force Base, MA.
- HAVSKOV, J., and OTTEMÖLLER, L. (2010), *Routine data processing in earthquake seismology*, Springer, Springer Dordrecht Heidelberg London New York, pp. 347.
- HOUSTON, H., BENZ, H.M., and VIDALE, J.E. (1998), *Time functions of deep earthquakes from broadband and short-period stacks*, *J. Geophys. Res.* 103, 29895–29913.
- HOUSTON, H. (2007), *Deep earthquakes*, in *Treatise on Geophysics*, Vol. 4: Deep Earthquakes, vol. 11, edited by G. Schubert, Elsevier, Amsterdam, The Netherlands, pp. 321–350.
- HUMPHREY, J.R., and ANDERSON, J.G. (1992), *Shear-wave attenuation and site response in Guerrero, Mexico*, *Bull. Seism. Soc. Am.* 81, 1622–1645.
- HUSSEINI, M.I. (1977), *Energy balance for formation along a fault*, *Geophys. J. R. Astr. Soc.* 49, 699–714.
- ICHINOSE, G.A., ANDERSON, J., SMITH, K., and YUEHUA, Z. (2003), *Source parameters of eastern California and western Nevada earthquakes from regional moment tensor inversion*, *Bull. Seism. Soc. Am.* 93, 61–84.
- ICHINOSE, G.A., ROMAN-NIEVES, J., and KRAFT, G. (2014), *Moment tensor inversion toolkit (MTINV) version 3.0.3 (software and manual)* <http://crackseismo.unr.edu/htdocs/students/Ichinose>.
- IDE, S., and BEROZA, G. (2001), *Does apparent stress vary with earthquake size?*, *Geophys. Res. Lett.* 28, 3349–3352. doi:10.1029/2001JB001617
- IDE, S., BEROZA, G., PREJEAN, S., and ELLSWORTH, W. (2003), *Apparent break in earthquake scaling because of path and site effects on deep borehole recordings*, *J. Geophys. Res.* 108, B5. doi:10.1029/2001JB001617.
- IGLESIAS, A., SINGH, S.K., PACHECO, J.F., and ORDAZ, M. (2003), *A source and wave propagation study of the Copalillo, Mexico earthquake of 21 July 2000 (M_w 5.9): Implications for seismic hazard in Mexico City from inslab earthquakes*, *Bull. Seism. Soc. Am.* 92, 1060–1071.
- JOST, M.L., and HERRMANN, R.B. (1989), *A student's guide to and review of moment tensors*, *Seism. Res. Lett.* 60, 37–57.
- KANAMORI, H., and ANDERSON, D. (1975), *Theoretical basis of some empirical relations in seismology*, *Bull. Seism. Soc. Am.* 65, 1072–1095.
- KANAMORI, H., ANDERSON, D.L., and HEATON, T.H. (1998), *Frictional melting during the rupture of the 1994 Bolivian earthquake*, *Science* 279, 839–842.
- KANE, D., PRIETO, G.A., VERNON, F.L., and SHEARER, P.M. (2011), *Quantifying seismic source parameter uncertainties*, *Bull. Seism. Soc. Am.* 101, 535–543.
- KEILIS-BOROK, V. (1959), *On estimation of the displacement in an earthquake source and of source dimensions*, *Ann. Geofis. (Rome)* 12, 205–214.
- KIKUCHI, M., and ISHIDA, M. (1993), *Source retrieval for deep local earthquakes with broadband records*, *Bull. Seism. Soc. Am.* 83, 1855–1870.
- KITA, S., and KATSUMATA K. (2015), *Stress drops for intermediate-depth intraslab earthquakes beneath Hokkaido, northern Japan: Differences between the subducting oceanic crust and mantle events*, *Geochem. Geophys. Geosyst.* 16, 552–562, doi:10.1002/2014GC005603.
- LAY, T., and BILEK, S. (2007), *Anomalous earthquake rupture at shallow depths on subduction zone megathrusts*, in *The Seismogenic zone of subduction thrust faults*, edited by T. H. Dixon and J.C. Moore, pp. 476–511, Columbia Univ. Press, New York.
- LUND, B., and TOWNEND, J. (2007), *Calculating horizontal stress orientations with full or partial knowledge of the tectonic stress tensor*, *Geophys. J. Int.* 270, 1328–1335.
- MAYEDA, K., and WALTER, W.R. (1996), *Moment, energy, stress drop, and source spectra of western United States earthquakes from regional coda envelopes*, *J. Geophys. Res.* 101, 11195–11208.
- MCGARR, A. (1999), *On relating apparent stress to the stress causing earthquake fault slip*, *J. Geophys. Res.* 104, 3003–3011.
- MINSON, S.E., and DREGER, D.S. (2008), *Stable solutions for complete moment tensors*, *Geophys. J. Int.* 174, 585–592. doi:10.1111/j.1365-246X.2008.03797.x.
- NAVA, F.A., TOLEDO, V., and LOMNITZ, C. (1985), *Plate waves and the 1980 Huajuapán de León, Mexico earthquake*, *Tectonophysics* 112, 46–492.
- ORDAZ, M., and SINGH, S.K., (1992), *Source spectra and spectral attenuation of seismic waves from Mexican earthquakes, and evidence of amplification in the hill zone of Mexico City*, *Bull. Seism. Soc. Am.* 82, 24–43.
- PACHECO, J.F., and SINGH, S.K. (2010), *Seismicity and state of stress in Guerrero segment of the Mexican subduction zone*, *J. Geophys. Res.* 115, B01303. doi:10.1029/2009JB006453.
- PAPAGEORGIOU, A.S., and AKI, K. (1983a), *A specific barrier model for the quantitative description of inhomogeneous faulting and the prediction of strong ground motion: I. Description of the model*, *Bull. Seism. Soc. Am.* 73, 693–722.
- PAPAGEORGIOU, A.S., and AKI, K. (1983b), *A specific barrier model for the quantitative description of inhomogeneous faulting and*

- the prediction of strong ground motion: II. Application of the model*, Bull. Seism. Soc. Am. 73, 953–978.
- PARDO, M., and SUÁREZ, G. (1995), *Shape of the subducted Rivera and Cocos plates in the southern Mexico: Seismic and tectonic implications*, J. Geophys. Res. 100, 12357–12373.
- PÉREZ-CAMPOS, X., and BEROZA, G. (2001), *An apparent mechanism dependence of radiated seismic energy*, J. Geophys. Res. 106, B6. doi:10.1029/2000JB900455.
- PÉREZ-CAMPOS, X., SINGH, S.K., and BEROZA, G.C. (2003), *Reconciling teleseismic and regional estimates of seismic energy*, Bull. Seism. Soc. Am. 93, 2123–2130.
- PÉREZ-CAMPOS, X., SINGH, S.K., IGLESIAS, A., ALCÁNTARA, L., ORDAZ, M., and LEGRAND, D. (2010), *Intraslab Mexican earthquakes of 27 April 2009 (M_w 5.8) and 22 May 2009 (M_w 5.6) and ground motion study*, Geofis. Internacional 49, 153–163.
- PRIETO, G.A., SHEARER, P.M., VERNON, F.L., and KILB, D. (2004), *Earthquake source scaling and self-similarity estimation from stacking P and S spectra*, J. Geophys. Res. 109, B08310. doi:10.1029/2004JB003084.
- PRIETO, G.A., FLOREZ, M., BARRET, S.A., BEROZA, G.C., PEDRAZA, P., BLANCO, J.F., and POVEDA, E. (2013), *Seismic evidence for thermal runaway during intermedite-depth earthquake rupture*, Geophys. Res. Lett. 40, 1–5. doi:10.1002/2013GL058109.
- RITSEMA, J., and LAY, T. (1995), *Long period regional waves moment tensor inversion for earthquakes in the western United States*, J. Geophys. Res. 100, 9853–9864.
- SINGH, S.K., and WYSS, M. (1976), *Source parameters of the Orizaba earthquake of August 28, 1973*, Geofis. Internacional 16, 165–184.
- SINGH, S.K., SUÁREZ, G., and DOMÍNGUEZ, T. (1985), *The great Oaxaca earthquake of 15 January 1931: lithosphere normal faulting in the subducted Cocos plate*, Nature 317, 56–58.
- SINGH, S.K., and ORDAZ, M. (1994), *Seismic energy release in Mexican subduction zone earthquakes*, Bull. Seism. Soc. Am. 84, 1533–1550.
- SINGH, S.K., PACHECO, J., COURBOULEX, F., KOSTOGLODOV, V., and SANTOYO, M.A. (1996), *Source duration of Mexican earthquakes*, Abs. Suppl. EOS, Trans AGU 77, 518.
- SINGH, S.K., ORDAZ, M., PACHECO, J.F., QUAAS, R., ALCÁNTARA, L., ALCOCER, S., GUTIERREZ, C., MELL, R., and OSVALDO, E. (1999), *A preliminary report on the Tehuacan, Mexico earthquake of 15 June, 1999 ($M_w = 7.0$)*, Seism. Res. Lett. 70, 489–504.
- SINGH, S.K., PACHECO, J.F., ORDAZ, M., and KOSTOGLODOV, V. (2000a), *Source time function and duration of Mexican earthquakes*, Bull. Seism. Soc. Am. 90, 468–482.
- SINGH, S.K., ORDAZ, M., ALCÁNTARA, L., SHAPIRO, N., KOSTOGLODOV, V., PACHECO, J.F., ALCOCER, S., GUTIERREZ, C., QUAAS, R., MIKUMO, T., and OSVALDO, E. (2000b), *The Oaxaca earthquake of September 30, 1999 ($M_w = 7.5$): a normal-faulting event in the subducted Cocos Plate*, Seism. Res. Lett. 71, 67–78.
- SINGH, S.K., ORDAZ, M., PACHECO, J.F., and COURBOULEX, F. (2000c), *A simple inversion scheme for displacement seismograms recorded at short distances*, J. Seism. 4, 267–284.
- SINGH, S.K., ORDAZ, M., PACHECO, J.F., ALCÁNTARA, L., IGLESIAS, A., ALCOCER, S., GARCÍA, D., PÉREZ-CAMPOS, X., VALDES, C., and ALMORA, D. (2007), *A report on the Atoyac, Mexico, earthquake of 13 April 2007 (M_w 5.9)*, Seism. Res. Lett. 78, 635–648.
- SINGH, S.K., PÉREZ-CAMPOS, X., ESPÍNDOLA, V.H., CRUZ-ATIEZA, V.M., and IGLESIAS, A. (2014), *Intraslab earthquake of 16 June 2013 (M_w 5.9) One of the closest such events to Mexico City*, Seism. Res. Lett. 85, 268–277.
- TIBI, R., BOCK, G., and WIENS, D.A. (2003), *Source characteristics of large deep earthquakes: constraint on the faulting mechanism at great depths*, J. Geophys. Res. 108, B2. doi:10.1029/2002JB001948.
- TOMIC, J., ABERCROMBIE, R.E., and DO NASCIMINETO, A.F. (2009), *Source parameters and rupture velocity of small $M \leq 2.1$ reservoir induced earthquakes*, Geophys. J. Int. 179, 1013–1023. doi:10.1111/j.1365-246X.2009.04233.x.
- UNAM Seismology group (2013), *Ometepec-Pinotepa Nacional, Mexico earthquake 2012 (M_w 7.5): A preliminary report*, Geofísica Int. 52, 173–193.
- VAVRYČUK, V. (2014), *Iterative joint inversion for stress and fault orientations from focal mechanisms*, Geophys. J. Int. 199, 69–77. doi:10.1093/gji/ggu224.
- VENKATARAMAN, A., and KANAMORI, H. (2004), *Observational constraints on the fracture energy of subduction zone earthquakes*, J. Geophys. Res. 109, B05302. doi:10.1029/2003JB002549.
- VIDALE, J., and HOUSTON, H. (1993), *The depth dependence of earthquake duration and implications for rupture mechanisms*, Nature 365, 45–47.
- YAGI, Y., and FUKAHATA, Y. (2011), *Introduction of uncertainty of Green's function into waveform inversion for seismic source processes*, Geophys. J. Int. 186, 711–720.
- YAMADA, T.J., MORI, J., IDE, S., KAWAKATA, H., IIO, Y., and OGASAWARA, H. (2005), *Radiation efficiency and apparent stress of small earthquakes in a South African gold mine*, J. Geophys. Res. 110, B01305. doi:10.1029/2004JB003221.
- YAMAMOTO, J., JIMENÉZ, Z., and MOTA, R. (1984), *El temblor de Huajuapán de León, Oaxaca, México, del 24 de octubre de (1980)*, Geofis. Internacional 23, 83–110.
- YOKOI, T., and IRIKURA, K. (1991), *Meaning of source controlled f_{max} in empirical Green's function technique based on a T^2 -scaling law*, Annuals of Disaster Prevention Research Institute, Kyoto University, vol. 34 B-1, 177–189.
- ZENG, Y., and ANDERSON, J. (1995), *A method for direct computation of the differential seismogram with respect to the velocity change in a layered elastic solid*, Bull. Seism. Soc. Am. 85, 300–307.